Diptera flight diversity is shaped by aerodynamic constraints, scaling, and evolutionary trade-offs

Camille Le Roy[1], Ilam Bharathi[1], Thomas Engels[2], and Florian T. Muijres[1*]

[1]**Experimental Zoology Group, Wageningen University, 6709 PG, Wageningen, the Netherlands.**
[2]**CNRS & Aix-Marseille Université, ISM, CEDEX 09, 13284 Marseille, France**
[*]Correspondence to: florian.muijres@wur.nl

ABSTRACT

Flight has been a key innovation in insect evolution, yet the selective and mechanistic forces shaping their flight motor systems remain poorly understood. Here, we present a comprehensive comparative analysis of Diptera (true flies), integrating morphology, wingbeat kinematics, and aerodynamics within a phylogenetic framework. We quantified morphology in 133 species spanning the Dipteran phylogenetic and size range, and for a subset of 46 species, we combined high-speed stereoscopic videography with computational fluid dynamics (CFD) to characterize wingbeat kinematics and aerodynamic performance, respectively. Our results reveal that morphology is strongly structured by phylogeny, whereas wingbeat kinematics are broadly conserved across Diptera, reflecting dominant aerodynamic constraints. Two basal lineages, Culicomorpha (mosquitoes and midges) and Tipulomorpha (crane flies), exhibit strikingly divergent kinematics and aerodynamics, suggesting lineage-specific selective pressures. Scaling analyses show that smaller species compensate for reduced aerodynamic force production efficacy through relatively larger wings, and higher wingbeat frequencies. Moreover, miniaturization is constrained by increased viscous drag at low Reynolds numbers, causing a plateau in aerodynamic power reduction with decreasing size. We further demonstrate that mosquitoes exhibit disproportionately high aerodynamic and acoustic power, coupled with enlarged flight musculature, consistent with sexual selection favoring acoustic signaling during in-swarm mating. This trade-off highlights how reproductive pressures can override aerodynamic efficiency. By integrating comparative morphology, kinematics, and aerodynamics across a major insect radiation, our study uncovers the interplay between physical scaling laws, aerodynamic constraints, and ecological pressures in shaping the evolution of animal flight. These findings provide a mechanistic framework for understanding how complex locomotor systems diversify under multiple selective forces.

Keywords: insect flight evolution; comparative biomechanics; wingbeat kinematics; wing morphology; aerodynamics; computational fluid dynamics; physical scaling

INTRODUCTION

Insects are the most species-rich group of animals, comprising an estimated 5 million species – about 80% of all known animal species (Grimaldi and Engel, 2005). Their remarkable radiation may be partly attributed to their flight ability (Nicholson et al., 2014), which has led to a striking diversity of aerial lifestyles (Dudley, 2002). Despite the pivotal role that flight has played in the evolution and ecological importance of insects, our understanding of the evolutionary processes that generate the diversity of their flight kinematics, morphology, and associated aerodynamics remains limited.

This is in part because insect flight is remarkably complex and challenging to quantify (Chin and Lentink, 2016), limiting the feasibility of large comparative evolutionary flight studies. While the flight of large vertebrate fliers can be addressed using classical aeronautical principles and often be inferred based on morphology (Rayner,

1988; Norberg, 2007; Baliga et al., 2019), that of insects heavily relies on complex high-frequency flapping wing motions, resulting in unsteady aerodynamic mechanisms that fall outside the realm of conventional aerodynamic theory (Srygley and Thomas, 2002; Sane, 2003; Chin and Lentink, 2016). Precisely quantifying the diversity of wing morphology and wingbeat kinematics as well as the underlying unsteady aerodynamics is therefore crucial to understand the evolution of flight in insects.

Fundamentally, flying insects generate aerodynamic forces through the reciprocal motion of the wings swept at a high angle-of-attack, but the overall wingbeat kinematics may greatly vary among taxa. The extent to which the evolution of wingbeat kinematics is channeled by aerodynamic constraints, and how these constraints mediate flight divergence between species, is poorly understood. Although bounded by physical laws, variations in wingbeat kinematics among flying insects can be influenced by distinct evolutionary pressure forces. On one hand, neutral divergence along phylogenetic tree branches may lead to different flight kinematics between species. On the other hand, selective pressures acting on flight can strongly influence the evolution of wingbeat kinematics, overcoming the pattern expected under neutral evolution.

Because flight is among the most energetically costly forms of locomotion (Norberg, 1996), minimizing its energetic demands may represent one of the strongest selective pressures shaping the insect flight motor system. Cost-reducing selective pressures may be especially strong in highly aerial species, such as long-distance migrants (Chapman et al., 2015). Conversely, adaptation to some ecological niche may promote the evolution of specialized flight abilities, leading to wingbeat kinematics that diverge from those predicted by energetic optimization alone. For example, the evolution of aerial predatory habits in some groups (e.g., dragonflies or robber flies) may promote adapted flight kinematics and morphology enabling extremely agile flight (Combes et al., 2012; Wardill et al., 2017). In contrast for prey species, natural selection may favor traits that enhance escape success, such as the rapid escape maneuverability of flies and mosquitoes (Muijres et al., 2014; Cribellier et al., 2024), or unpredictable flight behavior in mosquitoes and Lepidoptera (Jantzen and Eisner, 2008; Cribellier et al., 2022). Sexual selection may also exert a powerful influence on the evolution of flight. In hoverflies for example, maintaining a highly stable stationary flight is crucial for guarding a mating territory (Downes, 1969; Gilbert, 1984), which may drive the evolution of specialized hovering flight kinematics through male-male competition for females (Gilbert, 1984; Le Roy et al., 2025). Moreover, many insect species mate in large swarms, and in some of the swarming species, males locate females by detecting the auditory flight tones produced by their beating wings (Gupta et al., 2024; Belton, 1994; Downes, 1969). It has been suggested that the high-frequency wingbeat produced by swarming mosquitoes and midges (Culicomorpha) result from sexual selection, as it maximizes audibility during mating interactions (Gibson and Russell, 2006; Pennetier et al., 2010; Gupta et al., 2024).

Flying insects species span a impressive size range, from the tiniest 10 μg fairy-fly to the largest 100 g Goliath beetle, differing by seven orders of magnitude in body mass. Due to both physical and aerodynamic scaling laws, the mechanistic forces shaping the flight motor system can vary dramatically across these size ranges. For example, the Reynolds number, quantifying the relative importance of inertial and viscous forces on a moving object, differs substantially across animal sizes (Alexander, 2003), and consequently the flight style that minimizes energetic costs may also vary with size. The flight style minimizing energetic costs may thus also vary across size ranges. For example, tiny ptiliids beetles have evolved very lightweight bristled wings that yet still function effectively as solid surfaces at the low Reynolds numbers in which they operate (Farisenkov et al., 2022). In contrast, large flying insects, such as *Morpho* butterflies, experience Reynolds numbers high enough to permit efficient gliding, and have evolved wing shapes adapted for this flight mode (Le Roy et al., 2021).

The diversity of insect flight kinematics likely results from the interplay between shared ancestry, physical scaling laws, aerodynamic constraints, and ecological pressures. Disentangling the relative role of these factors on the evolution of such a complex trait is a major challenge necessitating a coupled comparative evolutionary, biomechanical and aerodynamic perspective. The integration of these approaches has nevertheless rarely been attempted.

Contrasting with the huge number of flying insect species, flight has been comprehensively studied in only a handful of them, mostly with the aim to understand the aerodynamic mechanisms involved (Willmott and Ellington, 1997; Lehmann and Dickinson, 1998; Ennos, 1989; Cheng et al., 2011; Muijres et al., 2014; Bomphrey et al., 2017; Aiello et al., 2021a). Although providing valuable insights into flight mechanics (Sane, 2003), such studies generally consider single (model) species, or at most few species in comparison, and are thus of limited evolutionary relevance. In contrast, more extensive comparative evolutionary studies on insect flight mostly focused on morphology only, or simple flight kinematics parameters such as wingbeat frequency, and simplified aerodynamic modeling (Byrne et al., 1988; Tercel et al., 2018; Dudley, 2002; Ellington, 1984c). This prevented us from fully appreciating the rich diversity in morphology, wingbeat kinematics and aerodynamics across taxa. The combination of detailed biomechanics studies and comparative phylogenetics is thus needed to understand the selective processes shaping the diversity of insect flight and associated morphologies.

To address this knowledge gap, we performed a broad-scale comparative study of detailed morphology, wingbeat kinematics and aerodynamics, focusing on the order Diptera (true flies). Flies represent one of the largest radiation of flying animals (Wiegmann et al., 2011). With approximately 160,000 named species spread across *ca.* 180 families (Wiegmann and Yeates, 2017), and an estimated >1 million undescribed species, they represent approximately 15% of all animal species (Grimaldi and Engel, 2005; Yeates and Wiegmann, 2005). Dipteran insects are found nearly everywhere on earth, inhabiting ecosystems ranging from the arctic tundras to the arid deserts (Danks and Oliver, 1972; Morgan and Shelly, 1988). They have been described as the ecologically most diverse animal order (Yeates et al., 2007), as they comprise a wide array of trophic specializations (including but not limited to saprophages, predators, blood-feeders, herbivores, or pollinivores), as well as highly diverse sexual behaviors among species (including swarming, mate guarding, or male-male territorial contest) (Kirk-Spriggs and Sinclair, 2017). Flight is central to many of Diptera's essential behaviors for survival and reproduction, making this group an ideal model for addressing the evolutionary and biomechanical drivers of flight diversity. The phylogenetic relationships are moreover relatively well-resolved for most Dipteran taxa (Yeates and Wiegmann, 2005; Lambkin et al., 2013; Wiegmann and Yeates, 2017), enabling to investigate the macro-evolutionary processes shaping trait diversity across species (e.g., Agrawal et al., 2017; Rohner, 2020; Yarger et al., 2021).

Diptera are regarded as highly-specialized fliers, with a remarkably sophisticated sensory-motor system. Their flight is powered by asynchronous indirect flight muscles that drive rapid wingbeats, while tiny steering muscles at the wing base provide precise flight control and steering (Deora et al., 2017; Melis et al., 2024). A other key trait in Diptera is the presence of halteres, which are specialized sensory and flight control organs derived from the hindwings (Nalbach, 1993; Agrawal et al., 2017). These club-shaped structures confer a precise control over body rotations during flight. The combination of specialized sensory and motor systems make Dipteran insects among the most agile flying animals (Deora et al., 2015; Melis et al., 2024).

Despite the high flight specialization of Diptera, marked differences in wingbeat kinematics exist among taxa. Most notably, the flight of mosquitoes (Culicidae) is characterized by low wingbeat amplitudes and high wingbeat frequencies (Bomphrey et al., 2017; Muijres et al., 2017a). In contrast, other similarly-sized Diptera such as fruit

flies (Drosophila) exhibit much larger wingbeat amplitude but lower frequencies (Lehmann and Dickinson, 1998). Moreover, mosquitoes exhibiting slender body forms and high-aspect-ratio wings, while fruit flies possess stouter bodies and low-aspect-ratio wings. In addition, the relative mass of flight musculature varies significantly between these taxa, from approximately 30% of total body mass in Drosophila to 55 % in Culicidae species (Lehmann and Dickinson, 1997; McLachlan and Neems, 1996), suggesting substantial variation in relative flight power availability. Mosquitoes and fruit flies thus represent two extremes in the diversity of Dipteran flight-motor systems. Beyond these two highly divergent species (phylogenetically basal vs. one of the most derived taxa, respectively), the evolution of flight kinematic in most other Dipterans remain largely unexplored, particularly regarding the interplay between aerodynamic constraints, energetic flight efficiency, and other selective pressures.

In this study, we aim to uncover the diversity of the flight motor system across the phylogeny of Diptera, and identify the evolutionary forces driving the underlying variations in morphology, flight kinematics, aerodynamics and energetic. For this, we quantified morphology, flight kinematics, and aerodynamic properties across a broad phylogenetic and size range of Diptera, and tested to what extent physical scaling laws and aerodynamic constraints explain variation in flight kinematics and energetics among species. Hereby, we focused on three key physical and physiological requirements for powered flight: generating sufficient aerodynamic force for weight support, minimizing aerodynamic power consumption, and the ability of flight muscles to deliver mechanical power. By contrasting theoretical expectations from physiological and aerodynamic models and the observed flight diversity, our work highlights how phylogeny, sexual selection, and ecological pressures influenced the evolution of the Dipteran flight motor system. These factors forced compromises between energetic flight efficiency and other selective demands, such as wingbeat-induced sound production for in-flight sexual communication.

MATERIAL AND METHODS

Sampling

We studied the diversity in flight motor systems among Diptera by collecting a total of 133 species, within 43 families spanning the phylogeny and size range of Diptera (Figs 1A and 1B, respectively). Most species (n=94) were captured in the surroundings of Wageningen University in the Netherlands (51°59’01.0”N 5°39’32.7”E; altitude ca. 10 m) during summer 2021 and 2022. An additional 36 species were sampled in the Amazonian rainforest of French Guiana (4°34’09”N 52°13’04”W, ca 300m) in July 2021, and three mosquitoes species were obtained from laboratory rearing. The mean$\pm$standard deviation of the number of species per family was 3.2$\pm$3.7, with 1.9$\pm$1.2 sampled individuals per species.

Species from the wild were identified through DNA barcoding. For this, we submitted leg samples from each individual to the Canadian Centre for DNA Barcoding (CCDB), where barcoding was performed using the standard automated protocols of the BOLD Identification System (http://www.boldsystems.org/) (Ratnasingham and Hebert, 2007). Comparison between the sequenced DNA and a reference library was then conducted to establish species matching. The number of individuals collected per species was too low to consider sexual differences. Sex of the collected flies was not determined, except for the mosquitoes with strong sexual dimorphism. We used the most comprehensive molecular phylogeny of Diptera (Wiegmann and Yeates, 2017) to build the phylogenetic tree for the 133 studied species of Diptera (Fig. 1A).

Although we aimed to maximize size diversity when capturing wild Dipterans, our sample was slightly biased toward larger species. This bias likely stems from the greater conspicuousness of larger individuals in the field,

making them easier to detect and capture. Nevertheless, the size distribution in our sample broadly captures the actual body size distribution across Diptera, as estimated from a large meta-analysis covering nearly 8,000 species (Ulrich and Szpila, 2008) (Fig. 1B).

For all studied species, we sampled the external body and wing morphology, and for a subset of 23 species (covering 11 families) we estimated the mass of their flight power musculature (Fig. 1C). For 46 species of Diptera (covering 30 families), we also captured the hovering flight kinematics using stereoscopic high-speed videography experiments, and we quantified the underlying fluid mechanics using Computational Fluid Mechanics (CFD) modeling and simulations.

For visualization, species were grouped by major lineages (infraorders or superfamilies, depending on the clade; see Fig. 1). Although these categories do not represent equivalent taxonomic ranks, they provide a practical way to convey broad phylogenetic positions across the studied species. All later described phylogenetic comparative analyses, however, were conducted at the species level.

Quantifying morphology

To quantify body and wing morphology, individuals were first euthanized by freezing them at -20°C. Masses of the animals and their body parts were measured using analytical balances. For insects and body parts larger than a fruit fly (m >0.3 mg), we used a balance with a resolution of 0.1 mg (XSR204 Mettler Toledo), while for smaller insects the balance had a resolution of 1 µg (Sartorius M2P). All measurements were performed within an hour after capture. Fresh body mass could not be directly measured for flies collected in French-Guiana. Therefore, we determined the relationship between dry and fresh body mass among all specimens collected in Wageningen as $m = 4.1 \cdot m_{\text{dry}} - 0.96$ (Fig. S1); we then estimated the fresh body mass of the specimens from French-Guiana based dry body masses using this relationship.

We quantified flight muscle mass on a subset of 23 species selected to span a broad phylogenetic and size range (Fig. 1A,C). For this, we dissected 5.0±1.2 thoraxes per species and weighed them immediately after separation from the body. Thorax of flying insects mainly contains flight muscle, which determines the power output for flight (Lehmann and Dickinson, 1997). Muscle mass, m_{muscle}, was thus estimated from that of the thorax, m_{thorax}, as $m_{\text{muscle}} = 0.9 \times m_{\text{thorax}}$ (Buchwald and Dudley, 2010).

Individual flies and their detached wings were photographed under a digital microscope (Zeiss Stemi SV11). From these photographs, body length and thorax width were first measured using ImageJ (Schindelin et al., 2012), and the body aspect ratio was computed as the ratio of body length to thorax width. We processed the wing images using WingImageProcessor in MATLAB (available at http://biomech.web.unc.edu/wing-image-analysis/), which provided us with estimates of the following wing morphology parameters (Fig. 2A): wing surface area S, wingspan b, and the wing second-moment-of-area relative to the wing hinge S_2. From these, we calculated the mean wing chord as $\bar{c} = S/b$, wing aspect ratio $\text{AR} = b/\bar{c} = b^2/S$, the radius-of-gyration of the flapping wing as $r_2 = \sqrt{S_2/S}$, and the span-normalized radius-of-gyration as $r_2^* = r_2/b$.

We quantified differences in wing shape among species in more detail using a landmark-based geometric morphometric approach (Bookstein, 1997). The outline of each wing was described with 300 semi-landmarks, equidistantly spaced along the wing outline. Semi-landmarks are used when identifiable landmarks are unavailable, typically to quantify curvy shapes. To align the wings, the semi-landmarks are sled along the curve to establish geometric correspondence by minimizing bending energy (see Gunz and Mitteroecker, 2013). After this alignment, the semi-landmarks are treated as regular ones in subsequent analyses. We did not consider vein architecture in

the analysis because the large phylogenetic scale of our study limits the number of homologous identifiable vein points between species. Nonetheless, one fixed landmark was placed at the wing hinge to fix the overall landmark configuration with respect to this homologous position available for all species. All landmarks were digitized using *TpsDig2* (Rohlf, 2015). Wing outlines were superimposed by performing a generalized procrustes analysis (Rohlf and Slice, 1990) using the *geomorph* R package (Adams et al., 2004). Through this process, the shape information is isolated by discarding the variations in size, position, and orientation. To analyse and visualize wing shape variation between the sampled Diptera species, we then performed a principal component analysis (PCA) on the superimposed coordinates. The evolutionary structure of Diptera wing shape diversity was visualized by superimposing the phylogenetic tree onto the morphospace (Fig. 2A).

Flight experiments

We studied the flight of 46 Diptera species (covering 30 families, Figs 1A and 3, Video S1), all collected in the surroundings of Wageningen University. Following capture in the wild, insects were brought in the laboratory for conducting the flight experiments. The experiments were performed in a custom-built octagonal flight arena with transparent Plexiglas walls (50 cm $\times$50 cm$\times$48 cm, height$\times$width$\times$length), adapted from Cribellier et al. (2022) (Fig. 3A). We placed three synchronized high-speed videography cameras (Photron FASTCAM SA-X2, operating at a spatial resolution of 1024$\times$1024 pixels, and an exposure time of 1/1000 s) around the arena to provide a top view, and inclined left and right side views of the flying insects. All three cameras were aimed at the center of the flight arena, where also their focal plane was positioned. We used infrared backlighting for camera illumination, by placing high-power infrared LED light panels (Osram OSLON Black Series (850 nm) 150°, SFH 4716A) behind the bottom and lower side walls of the octagonal arena, opposite each camera (Fig. 3A).

For the experiments, we used two videography configurations, a zoomed-in and zoomed-out configuration for the smaller and larger insects, respectively. For species with body lengths larger than approximately 3 mm, we equipped the cameras with Nikon Sigma 135 mm lenses, resulting in a focal zone of approximately 12$\times$12$\times$12 cm in the center of the arena in which the insect was in focus of all three cameras. For smaller species cameras were equipped with Canon EF 100–400mm lenses paired with a 2$\times$ extender (effective focal length: 200–800mm), resulting in an approximate focal zone of 6$\times$6$\times$6 cm.

We adapted camera frame rate based on the wingbeat frequency of the specific flying insect, by aiming to recorded at least 20 video frames per wingbeat for proper wingbeat kinematics reconstruction. In addition, we used a minimum frame rate of 5000 frames s^{-1} for the low-frequency flyers (e.g. crane flies), and the maximum frame rate achievable by the cameras (13 500 frames s^{-1}) for high-frequency flyers (e.g. mosquitoes).

Before each flight experiment, we calibrated the stereoscopic camera system using the Direct Linear Transformation (DLT) method (Hartley and Sturm, 1995), within the MATLAB program easyWand (Theriault et al., 2014). For this, we used a T-shaped wand with a ball on each end of the T-crossbar that we manually moved within the focal zone of the cameras. The crossbar-ball distance was 2.8 cm and 1.0 cm for the zoomed-out and zoomed-in configuration, respectively. We tracked the position of both balls using an artificial neural network trained with the pose estimation Python library DeepLabCut (Nath et al., 2019). Calculation of the DLT coefficients was then done using the MATLAB program easyWand (Theriault et al., 2014).

During a flight experiment, several individuals of the same species were simultaneously released in the arena to increase the chance of an individual insect flying through the focal zone in the center of the arena. When this would occur, the camera system was manually triggered using an end-trigger, thereby storing the video buffer recorded

preceding the trigger moment. For each species, filming continued until a minimum of three flight sequences were captured. While this procedure facilitated data collection, it precluded the identification of specific individuals in flight, thus allowing for the potential recording of the same individual on multiple occasions. Because direct assignment of flight measurements at the individual level were thus not possible, we here aimed at determining the average wingbeat kinematics per species instead of per individual. After the flight experiment, all insects within the arena were euthanized, and their morphological characteristics were measured following the method described in the previous section.

Quantifying body and wingbeat kinematics

We quantified the body and wingbeat kinematics of all recorded flight sequences using an adaptation of the manual stereoscopic video tracker *Kine* in MATLAB (Fry et al., 2003; Fontaine et al., 2009), originally developed for tracking the wingbeat kinematics of flying fruit flies. Here, we adapted the tracker by building wing models matching the wings of each studied species. These wing models were constructed by digitizing the wing outline from digital microscope photographs, resulting in 41 2D coordinates representing the shape of the wing outline, including the known hinge and tip positions. The tracking method is based on a rigid flat wing model, and thus wing deformations were ignored.

The body and wingbeat kinematics were tracked on videos comprising 34.6±7.7 frames (mean±s.d.) per wingbeat. To speed up digitization, videos were down-sampled for low-frequency flyers, to 2500 frames s^{-1} at its lowest. Through tracking, we acquired the position and orientation of the body and wings in each consecutive video frame, using the conventions described in Muijres (2023) (Fig. 3A). The position and orientation of the body were defined in the world reference frame, as the temporal dynamics of the three-dimensional position vector ($\mathbf{X} = [x, y, z]$, where the z-axis points vertically up), and the consecutive Euler angles body yaw ψ, body pitch β, and body roll φ. The angular orientations of the wings throughout the wingbeats were expressed in the stroke-plane coordinate system, using three Euler angles Muijres (2023) (Fig. 3A). In consecutive order, these are: the stroke angle (ϕ), defined as wing hinge rotations within the stroke-plane; deviation angle (η), defined as rotations out of the stroke-plane; rotation angle (θ) , defined as wing rotations along the spanwise axis (Fig. 3B).

The stroke-plane was defined as a plane fixed within the body reference frame, located at the wing hinge positions, and within which the majority of wingbeat motions were executed. Because the wing deviation angle is defined as angular rotations out of the stroke-plane, this means that the stroke-plane is defined as the plane for which the wing deviation movements are minimal. The stroke-plane orientation is characterized using its pitch angle relative to the horizontal. We measured this stroke-plane pitch angle $\beta_{\text{stroke-plane}}$ by estimating the pitch angle for which the wingbeat-average deviation angle was minimal, using a Nelder-Mead optimization algorithm (Gao and Han, 2012) of the Scipy python package.

The wingbeat kinematics were tracked for the left and right wings separately, and then averaged between the two wings. The time history of the averaged wing kinematics angles were then fitted with a 4th-order Fourier series for all three angles (Muijres et al., 2014). From this, we computed the wingbeat frequency as $f = 1/\Delta T$, where ΔT equals the time between consecutive wingbeats, and wingstroke amplitude as $A_\phi = \phi_{\max} - \phi_{\min}$, where $\phi_{\max}$ and $\phi_{\min}$ are the maximum and minimum stroke angle within the average wingbeat, respectively. We estimated the angle of attack (α) as the angle between the wing surface and its wingbeat-induced velocity vector (Fig. 3A). We calculated the time derivatives of the wingbeat kinematics angles (i.e. stroke, deviation and rotation rate) analytically from the respective Fourier series. From these, we then estimated the angular speed of the beating wings as $\omega = \sqrt{\dot{\phi}^2 + \dot{\eta}^2}$,

where $\dot{\phi}$ and $\dot{\eta}$ are the stroke rate and deviation rate, respectively.

We quantified the body kinematics during each wingbeat using the wingbeat-average flight speed, climb angle, and body pitch angle. For this, we first determined the temporal dynamics of flight velocity $\mathbf{U}(t)$ as the temporal derivative of body positions. From this we estimated the mean flight speed U as the wingbeat-average magnitude of flight velocity, and the corresponding climb angle as $\gamma_{\text{climb}} = \text{atan}(U_{\text{ver}}/U_{\text{hor}})$. Here, U_{ver} and U_{hor} are the wingbeat-average vertical and horizontal component of flight velocity. Body pitch angle β_{body} was calculated as the angle between the body axis and the horizontal.

We assessed to what extent the studied wingbeat were representative for hovering flight by computing the advance ratio of all wingbeats as $J = U/(\bar{\omega}\, b)$, where $\bar{\omega}$ is the wingbeat-average angular wing speed. Hovering is generally defined as flight with advance ratios $J < 0.1$, i.e. when the forward flight speed is less than 10% of the wingbeat-induced speed of the wingtip (Ellington, 1984a).

Because variability in flight measurements is typically high, especially in comparison to morphological measurements, we assessed the robustness of species-level differences in flight traits. For this, we compared within-species and between-species variation in each parameter to verify that our experiment effectively captured difference in flight kinematics between species. We applied a nested ANOVA model in which flight sequence replicate was nested within species as a random effect. Comparison of sum of squares allowed assessing the variance attributable to differences between species versus within species. To facilitate the visual comparison of interspecific versus intraspecific variation across parameters, we also computed the coefficient of variation for each parameter as $C_{\text{var}} = \frac{\text{SD}}{\text{mean}} \times 100\%$ (Fig. S2).

Assessing the influence of phylogeny on morphological and flight traits

To evaluate whether shared evolutionary history among Dipteran species influenced variation in morphology and wingbeat kinematics, we tested if closely related species showed more similar values in the measured parameters than distantly related ones. This was done by calculating the phylogenetic signal with Blomberg's K-statistics (Blomberg et al., 2003) on each flight and morphological parameter using the *phytools* R package (Revell, 2012). Additionally, the multivariate generalization of Blomberg's K (Adams, 2014) was computed separately for the combined variation in morphological parameters, and combined variation in flight parameters. Tests were performed using the most comprehensive molecular phylogeny of Diptera (Wiegmann and Yeates, 2017) that was pruned to the species studied here, i.e., 133 species for the morphological dataset and 46 species for the flight dataset (Fig. 1A).

Computational fluid dynamics simulations

To estimate the aerodynamic forces and torques generated during hovering flight of the studied Diptera species, we performed Computational Fluid Dynamics (CFD) simulations. For each simulation, we modeled a single rigid, flat wing, using species-specific contours and wingbeat kinematics. The computational domain measured $10b \times 10b \times 10b$, and three complete wingbeat cycles were simulated. The wing thickness was set to 0.025 b. Assuming hovering flight conditions, we did not impose any mean inflow into the domain ($U_\infty = 0$).

The simulations were carried out using our in-house open-source code WABBIT (Wavelet Adaptive Block-Based solver for Insects in Turbulence, see Engels et al., 2021, 2022). This computational framework utilizes explicit finite difference methods to solve the incompressible Navier–Stokes equations under an artificial compressibility approach. Dynamic grid adaptation is achieved through wavelets, enabling local refinement of the discretization grid based on the flow at each time step. This ensures computational resources are allocated efficiently, with higher refinement

where needed and coarser grids in regions of lesser importance. Starting from a coarse base grid, we allowed up to seven refinement levels, with each level doubling the grid's resolution. A Cohen-Daubechies-Feauveau wavelet (CDF60) was employed, and each block in the grid contained $B_s = 24$ points per spatial direction, leading to an effective maximum resolution of 307 points per wing radius (b). An additional simulation using eight refinement levels verified the accuracy of the results. As shown in prior validation tests, the numerical results are considered quasi-exact, equivalent to a physical experiment with the same rigid geometry and kinematics. For further details on the code, see Engels et al. (2021). The necessary parameter files to replicate these simulations are available in the supplementary materials. To optimize performance, each simulation used up to 600 CPU cores and up to 2.7 TB of memory.

Modeling the aerodynamics and aeroacoustics of Diptera flight

Generating enough lift to stay in the air and minimizing the energy needed to do so are key aerodynamic constraints governing animal flight (Alexander, 2003). Moreover, selective pressures acting on sound production – such as in some swarming insect species – may affect the evolution of wingbeat kinematics (Seo et al., 2019). To understand how these constraints shapes the evolution of Diptera's flight, we integrated our wingbeat kinematics and morphological data into models of aerodynamic force production, as well as aerodynamic and acoustic power.

Aerodynamic force production by flapping insect wings

We modeled the aerodynamic force produced by flapping wings through CFD simulations, employing dynamic scaling. This approach was also used to investigate the effect of wing morphology and wingbeat kinematics on aerodynamic force production. We performed dimensional analyses following Buckingham-Pi theorem, which identifies key non-dimensional variables governing the system (Barenblatt, 2003). This allowed us to determine the minimal set of dimensional and non-dimensional parameters governing aerodynamic force production. From our dimensional analysis (see supplementary text for detail), the aerodynamic forces produced by a beating wing scale as

$$F = \rho\ f^2\ b^4\ K \tag{1}$$

where ρ is air density, f is the wingbeat frequency, b is the wingspan, and K is a parameter that includes all additional non-dimensional quantities related to the wing morphology, wingbeat kinematics, and aerodynamics.

For the rotational movements of flapping insect wings, the primary non-dimensional kinematic parameters include wingbeat amplitude A_ϕ and the angle-of-attack α (Ellington, 1984a). The primary non-dimensional morphological parameters are the wing aspect-ratio AR and the non-dimensional radius of gyration r_2^*. The primary non-dimensional aerodynamics parameter is the so-called aerodynamic force coefficient C_F, which depends primarily on the angle-of-attack of the wing α and the Reynolds number defined as $\mathrm{Re} = U_r\ \bar{c}/\upsilon$, where U_r is the wingbeat-average speed of the wing and υ is the kinematic viscosity of air.

The aerodynamic force produced by a beating wing scales linearly with the product of the dynamic pressure and wing surface area as $F \sim q\ S$, where the dynamic pressure equals $q = 1/2\ \rho U_r^2$. Here, the mean wingbeat-induced speed of the wing scales with the primary (non)dimensional morphological and kinematics parameters as $U_r = b\ r_2^*\ f\ A_\phi$; representing the average wing speed at the radius of gyration. The wing surface area can similarly be converted to the primary morphological (non)dimensional parameters as $S = b\bar{c} = b^2/\mathrm{AR}$. Substituting these into equation 1 results in the following scaling relationships for the wingbeat-average aerodynamic force produced by a

flapping wing

$$\mathbf{F} = 1/2\,\rho\,U_r^2\,S\,C_F = \frac{\rho\,r_2^{*2}\,b^4}{2\,\mathrm{AR}}\,(fA_\phi)^2\,C_F\ , \tag{2}$$

where **F** = (L,D) and $C_F = (C_L, C_D)$ are the respective force and coefficient vectors for lift L and drag D. This scaling relationship can be used to understand the relative effect of wing size (b), wing shape (AR and r_2^*), wingbeat kinematics (f and A_ϕ) and aerodynamics (C_F) on aerodynamic force production across Diptera species.

Because we assume hovering flight, here we focus primarily on vertical force production for weight support $F_V = mg/2$, where F_V is the vertical force produced by a single wing and g equals gravitational acceleration. Thus, by replacing F and C_F with their vertical components (F_V and C_V), and normalizing with $mg/2$, the weight-normalized wingbeat-average vertical force F_V^* scales as

$$F_V^* = \frac{\rho\,r_2^{*2}\,b^4}{mg\,\mathrm{AR}}\,(fA_\phi)^2\,C_V. \tag{3}$$

To test the validity of this scaling in the context of our work, we compared the vertical force coefficients from our model with those derived from CFD. After validating our model, we used it to estimate how Diptera of different sizes and morphologies produce weight-support during hovering flight.

Aerodynamic power for flight

Beyond producing sufficient lift for weight support, selection for minimizing energy expenditure may have favored traits reducing flight cost. To assess how energy-minimization affects wingbeat kinematics and morphology in Diptera, we modeled the aerodynamic power required for flight using both CFD and the dimensional analyses. The aerodynamic power required for Diptera flight equals the dot product of the aerodynamic torque on a single wing ($\mathbf{T}_{\mathrm{aero}}$) and the angular velocity of that wing (Ω) as

$$P_{\mathrm{aero}} = 2\,\mathbf{T}_{\mathrm{aero}} \cdot \Omega. \tag{4}$$

Using this equation, we estimated the wingbeat-average aerodynamic power for all 46 species studied using CFD. We then normalized this aerodynamic power with the aerodynamic force magnitude as $P_{\mathrm{aero}}^* = P_{\mathrm{aero}}/|F|$. In hovering flight the aerodynamic force magnitude should equal body weight, and thus we will refer to this parameter as the weight-normalized aerodynamic power.

To investigate how differences in in morphology, wingbeat kinematics and aerodynamic properties contribute to power variation across Diptera species, we further employed dimensional analysis. For this, we reduced equation 4 to include the primary dimensional parameters. Assuming that aerodynamic power is primarily used to overcome drag force D, the aerodynamic torque simplifies to the scalar form $T_{\mathrm{aero}} = D\,r_D^*\,b$, where r_D^* is the span-normalized moment arm of the drag force vector (Lyu and Sun, 2021). The angular velocity vector Ω reduces similarly to the angular speed scalar ω, which itself scales with the product of wingbeat frequency and amplitude ($\omega \sim f\,A_\phi$). As a result, the scaling of the wingbeat-average weight-normalized aerodynamic power with morphology, kinematics and aerodynamics is

$$P_{\mathrm{aero}}^* \sim r_D^*\,b\,f\,A_\phi\,D^* \sim U_D\,D^*, \tag{5}$$

where $D^* = D/mg$ equals the mean weight-normalized drag force acting on the beating wing, and U_D equals the average wingbeat-induced wing speed at the drag force moment arm.

In hovering flight ($F_V = mg$) the weight-normalized drag force equals the ratio between the vertical force coefficients and the drag force coefficients of the beating wing ($D^* = C_D/C_V$). The inverse of this ratio is similar to the well-known lift-to-drag ratio of a wing (C_L/C_D), which is a flight efficiency parameter that depends on the wing angle-of-attack and Reynolds number (Broadley and Nabawy, 2022; Lyu et al., 2019). The weight-normalized drag force thus describes an equivalent aerodynamic cost for flight, as it depicts the relative amount of aerodynamic drag produced in hovering flight. Here, we use $D^* = C_D/C_V$ instead of the inverse of C_L/C_D because several species of Diptera tend to have an inclined stroke-plane during hovering, resulting in a misalignment between the lift force (normal to the stroke-plane) and vertical force for weight support. Note that for a horizontal stroke-plane, C_V/C_D reduces to C_L/C_D.

To test the validity of this simplified aerodynamic power model, we compared its output with the power estimated from CFD, for all Diptera species studied using CFD. After this validation, we used the model to assess the respective impact of wing size (b), wing shape (r_D^*), wingbeat kinematics (f and A_ϕ), and aerodynamics (D^*, C_V, C_D) on the required aerodynamic power for hovering flight across Diptera.

Acoustic power produced by flapping wings

Many Diptera species mate on the wing in swarms (Nielsen and Haeger, 1960), but in mosquitoes and midges acoustic communication plays a central role, with males and females locating conspecifics using the sound generated by their beating wings (Pennetier et al., 2010). This mating system may have promoted the evolution of wingbeat kinematics that generate high acoustic power (Seo et al., 2019), potentially at the expense of an increase in the aerodynamic power required for flight (Liu et al., 2024). To test whether this mate-location behavior, which promotes enhanced sound production, has compromised flight energetic efficiency, we modeled the in-flight acoustic power in Diptera using both CFD simulations and dynamic scaling.

When flapping their wings, flying insects produce sound via pressure fluctuations due to air disturbances. Such aerodynamically generated sound can be decomposed by its directivity as monopoles, dipoles, and quadrupoles (Ffowcs Williams and Hawkings, 1969). These correspond to fluctuations in mass, force, and advective stresses, respectively. Insect wings being thin and operating at low Reynolds numbers, where turbulence is minimal, we can assume that sound production primarily arises from fluctuations in aerodynamic forces(Lighthill, 2001; Nedunchezian et al., 2019). Because the speed of sound far exceeds wing speed, dipole pressure fluctuations at a given location and time, far from the sound source, can be represented by (Hirschberg and Rienstra, 2004)

$$p'(\mathbf{X},t) \approx \frac{1}{4\pi r c_s} \frac{\mathbf{x}_i}{r} \frac{\partial \mathbf{F}_i(t')}{\partial t} \tag{6}$$

where r is the radial distance from the source, c_s is the speed of sound in air, $\mathbf{x}_i/r$ represents the directionality of sound, and $t' = t - f\ r/c_s$ is the retention time, representing the time it takes for the sound to propagate from the source to the observer. Assuming that sound production is governed primarily by pressure and neglecting both the effect of wing orientation and the time it takes for sound to travel to the observer, the sound pressure can be modeled as

$$p'(\mathbf{X},t) \approx \frac{1}{4\pi\ r c_s} \frac{\partial \mathbf{F}_p}{\partial t}, \tag{7}$$

where F_p is the pressure force on the sound-producing wing. In the field far from the source, the acoustic power is then defined as

$$P_{\text{acoustic}} = \int \frac{\overline{p'^2}}{\rho c_s} dA_{\text{sphere}} = \frac{1}{4\pi\,\rho\,c_s^3} \overline{\left(\frac{\partial \mathbf{F}_p}{\partial t}\right)^2} = \frac{g^2}{\pi\,\rho\,c_s^3} \left(\overline{\frac{\partial C_p}{\partial t^*}} \frac{1}{C_V}\right)^2 m^2 f^2, \tag{8}$$

where $t^* = 1/f$ is the wingbeat cycle period.

This equation indicates that the primary dimensional determinants of acoustic power are the wingbeat frequency and body mass of the animal. In contrast, the vertical aerodynamic force in insect flight scales with the product of wingbeat frequency and amplitude as $F_V \sim (f\,A_\phi)^2$. Thus, flying insects can maximize their acoustic efficiency while maintaining weight-support ($F_V = mg$), by simultaneously increasing wingbeat frequency and decreasing wingbeat amplitude.

To separate the relative effect of wingbeat kinematics and aerodynamics on aero-acoustic sound production, we defined the normalized acoustic power as

$$P^*_{\text{acoustic}} = \left(\overline{\frac{\partial C_p}{\partial t^*}} \frac{1}{C_V}\right)^2 = \frac{\pi\,\rho\,c_s^3}{(mg\,f)^2}\,P_{\text{acoustic}}. \tag{9}$$

This parameter equals the square of the ratio between the aerodynamic pressure fluctuations that result in sound production ($\overline{\frac{\partial C_p}{\partial t^*}}$) and the vertical aerodynamic force required for in-hovering weight-support (C_V). It thus quantifies the relative sound production per unit of aerodynamic force production, during hovering flight.

We used the above-described acoustic model to assess whether Diptera that use in-flight acoustic communication for mate-location have evolved more efficient wingbeat-induced sound production, and whether this comes at the cost of reduced aerodynamic efficiency. In addition, we used the model to identify how adaptations in morphology (b, AR and r_2^*), kinematic (f and A_ϕ) and aerodynamic (D^* and $\partial C_p/\partial t^*$) that enhance sound production in Diptera.

Estimating flight power from muscle morphology

We compared the previously estimated required aerodynamic power for flight (P^*_{aero}) with the power available in the flight musculature ($P_{\text{available}}$). Available power was estimated as

$$P_{\text{available}} = P^*_{\text{muscle}} \cdot m_{\text{muscle}} \tag{10}$$

where m_{muscle} is the flight muscle mass, and P^*_{muscle} is the mass-specific, wingbeat cycle-averaged power output per kilogram of muscle. We used a value of $P^*_{\text{muscle}} \sim 100$ W/kg, consistent with previous studies reporting a relatively narrow range of 80–120 W/kg across insect taxa and body sizes (Gilmour and Ellington, 1993; Lehmann and Dickinson, 1997; Josephson et al., 2000). As described above, we estimated the flight muscle masses based on thorax mass (Lehmann and Dickinson, 1997). We then tested whether interspecific differences in power requirements were matched by corresponding variation in available power using a PGLS regression.

Adaptations in morphology, wingbeat kinematics and aerodynamics across the Diptera phylogeny

We studied how variations in morphology, wingbeat kinematics and aerodynamics across the Diptera phylogeny, contribute to achieving weight support, minimizing aerodynamic power of flight, and maximizing wingbeat-induced

sound production for in-flight communication. We did so using our dynamic scaling models for aerodynamic force and power production (Eqns 3 and 6, respectively), and our acoustic power model (Eqn 9).

Scaling of aerodynamic force production with body mass

For an animal to stay aloft during hovering flight, the aerodynamic thrust force should be directed vertically upwards and equal to the weight of the animal. Thus, to maintain weight support among different sizes of Diptera, the aerodynamic force should scale linearly with body mass. This cannot be achieved when geometric, kinematic, and dynamic similarity are preserved across sizes. Here, we refer to geometric similarity across size as isometric scaling of body and wing morphology (e.g. b, AR and r_2^*), kinematic similarity as maintaining the same wingbeat kinematics across size (f, A_ϕ, α, etc), and dynamic similarity when fluid dynamic characteristics are maintained (e.g. constant Re, D^*, C_V and C_D).

For isometric scaling of morphology, the parameters of interest scale with body mass as $b \sim m^{1/3}$, $r_2^* \sim m^0$, AR $\sim m^0$. For kinematic similarity across sizes, all wingbeat kinematics parameters of interest are per definition independent of body mass ($f \sim m^0$, $A_\phi \sim m^0$, $\alpha \sim m^0$). The combined morphological and kinematics parameter wingbeat-induced wing speed should scale under similarity as $U_r \sim m^{1/3}$. Finally, for dynamic similarity across sizes, the aerodynamic force coefficients would also be independent of body mass ($C_V \sim m^0$).

Thus, for the hypothetical case of geometric, kinematic and dynamic similarity across sizes of Diptera, the vertical aerodynamic force for weight support scales with body mass as $F_V \sim m^{4/3}$ (Eqn 3; see supplementary text for details). This scaling factor is larger than one, and so with an isometric reduction in size, the aerodynamic force for weight support reduces more quickly than body mass. This shows that, compared to large species of Diptera, small species need relatively larger wings (negative allometry), or adjust their wingbeat kinematics to maintain weight support.

Using our aerodynamic force model (Eqn 3), we can predict how wing morphology or wingbeat kinematics should scale allometrically with body mass to maintain weight support across the Dipteran size range ($F_V \sim m^1$). Diptera of different sizes can, and most likely do, maintain this linear scaling of the vertical force with body mass by combined adaptations in morphology and wingbeat kinematics. Here, we define the extreme scenarios in which weight support is maintained across sizes, by allometric scaling of only a single parameter in equation 3. In such scenario, the various parameters should scale with mass as either $b \sim m^{1/4}$, $r_2^* \sim m^{-1/6}$, AR $\sim m^{1/3}$, $f \sim m^{-1/6}$, $A_\phi \sim m^{-1/6}$, $U_r \sim m^{1/6}$ or $C_V \sim m^{-1/3}$ (see supplementary text for details).

We assessed how morphology, kinematics and aerodynamics scale with body mass for hovering Diptera, while accounting for phylogenetic distance between species, using Phylogenetic Generalized Least Squares (PGLS) regressions (Symonds and Blomberg, 2014) on $\log_{10}$-transformed variables. For each measured parameter, we evaluated whether the observed slope significantly deviated from the slopes for geometric, kinematic and dynamic similarity by verifying if its 95% confidence intervals excluded this similarity slope (see Table 1 and supplementary text for isometric slope assumptions on the different parameters).

Finally, we assessed the relative contribution of morphological and kinematic traits in producing weight support across Diptera, using the fitted scaling factors. To do this, we first calculated for all relevant parameters the difference between the observed allometric scaling factor and the scaling factor for similarity, as $\Delta a = (a_{\text{allo}} - a_{\text{sim}})$. We then calculated the proportional contributions of the i-th parameter to the overall allometric deviation from similarity as

$$a^*_{\text{allo},i} = \frac{n_i \, \Delta a_i}{\sum n_j \, \Delta a_j} \cdot 100\%. \tag{11}$$

Here n_i equals the power scaling of parameter i in the force scaling model (Eqn 3), and $j = [1 : J]$ is the set of all independent parameters in Eqn 3. This metric thus quantifies the relative contribution of allometric adaptations in all relevant traits to maintaining weight support across sizes.

Assessing the role of cost minimization in Diptera flight

Flight is one of the most energetically costly mode of locomotion, with the highest energy expenditure per unit time (Norberg, 1996). The evolution of morphological and kinematic traits is thus expected to be highly constrained by demands on costs minimization, with strong selection exerted on morphology, flight kinematics and aerodynamics, for reducing energy expenditure.

To assess the extend to which cost minimization explains the diversity of flight among Diptera, we used our scaling model for aerodynamic power (Eqns 4-6) to examine whether Diptera flight minimizes aerodynamic power relative to body mass. According to this model, the weight-normalized aerodynamic power for hovering flight scales linear with the product of wingbeat-induced speed and normalized drag as

$$P^*_{\text{aero}} \sim U_D \, D^*. \tag{12}$$

To maintain weight support during hovering flight, this wing speed should scale with body mass as $U_D \sim m^{1/6}$. Thus, when assuming dynamic similarity ($D^* \sim m^0$), weight-normalized aerodynamic power should also scale with body mass as $P^*_{\text{aero}} \sim m^{1/6}$.

Across the size range of Diptera, the assumption of dynamic similarity ($D^* \sim m^0$) is most likely not valid, particularly due to the scaling of drag forces with Reynolds number (Hoerner, 1965). The Reynolds number defines the relative contribution of inertia and viscosity to aerodynamic (drag) force production, and thus with increasing Re the relative drag D^* is expected to decrease due to reduced viscous drag.

In the intermediate Reynolds number regime at which Diptera operate ($\text{Re} \sim 10^1 - 10^4$), the dependency of airfoil drag on Reynolds number changes drastically. In steady flow conditions at low Reynolds numbers ($\text{Re} < 300$), drag scales with Reynolds number as $C_D \sim \text{Re}^{1/2}$ due to strong viscous effects. At Reynolds numbers greater than 300, the viscous effects quickly decrease and drag becomes approximately independent of the Reynolds number ($C_D \sim \text{Re}^0$)(Schlichting and Gersten, 2016). A similar trend of drag with respect to Reynolds number has been observed in a parametric study on insect wing aerodynamics (Lyu et al., 2019). This suggests that tiny Diptera operating at Re<300 should require increased aerodynamic power for flight due a Reynolds-number dependent increase in relative drag, whereas for larger Diptera the Reynolds-number effect on relative drag is negligible.

We tested whether weight-normalized aerodynamic power scales with body mass according to both physical scaling laws ($U_D \sim m^{1/6}$) and aerodynamic scaling ($D^* \sim 1/\text{Re}$ at low Reynolds numbers). We did so by first determining the weight-normalized aerodynamic power P^*_{aero} and relative drag D^* from CFD, for each CFD-studied Diptera species. Then, we compared the true weight-normalized aerodynamic power with the model predictions. Finally, we tested whether the sub-components of the aerodynamic power model (U_D and D^*; Eqn 5) scale with size according to the hypothesized physical and aerodynamic scaling laws, respectively.

Scaling of aero-acoustic power with body mass and aerodynamic efficiency

Finally, we assessed whether Diptera species that use in-flight acoustic communication in mating swarms have evolved more efficient wingbeat-induced sound production, and whether this comes at the cost of reduced aerodynamic efficiency. For this, we estimated aero-acoustic power for each studied Diptera using our acoustic model

applied to our CFD results.

Based on this, we first tested how the acoustic power scales with body mass, by correlating acoustic power with body mass using a PGLS regression. According to equation 8, the acoustic power scales as $P_{\text{acoustic}} \sim m^2 f^2$. To maintain weight-support across sizes through adaptations in wingbeat frequency only (isometric scaling), wingbeat frequency should scale with mass as $f \sim m^{-1/6}$. Thus, in these conditions, acoustic power would scale with body mass as $P_{\text{acoustic}} \sim m^{5/3}$ (see Supplementary Information for details). We therefore tested whether the PGLS regression on acoustic power versus body mass differed significantly from this isometric scaling.

Second, we tested whether any increase in acoustic power corresponds to a rise in relative aerodynamic drag during hovering flight. For this, we first estimated the non-dimensional relative acoustic power P^*_{acoustic} using the CFD-derived acoustic power, in combination with the measured kinematics and wing morphology data (Eqn. 9). We then used a PGLS regression to test how this relative acoustic power P^*_{acoustic} scaled with the aerodynamic cost parameter D^*. Finally, we compared the combined results between Diptera species that rely on acoustic signals for mate-localization and those that do not.

RESULTS

Morphological and kinematic diversity in Diptera

We investigated morphological diversity across 133 Diptera species and flight kinematic diversity in a subset of 46 species (Fig. 1, Video S1). For this, we quantified the body and wing morphology of 220 individual insects (mean±standard deviation = 1.9±1.2 individuals per species), and the body and wingbeat kinematics throughout 138 wingbeats in 46 Diptera species (3 wingbeats per species). The species studied broadly covered the phylogenetic tree (Fig. 1A), and a large range of body masses, from 0.02 mg (*Micromya lucorum*, Cecidomyiidae) to 227 mg (*Tabanus sp.*, Tabanidae) (Fig. 1B).

Morphological diversity in Diptera

Our geometric morphometrics analysis revealed that wing elongation represents the primary axis of variation in the wing shape morphospace, accounting for 75% of the total shape variation (PC1 Fig. 2A). Wing elongation differentiates the major dipteran groups well: more basal lineages exhibit elongated wings (negative PC1 values), whereas more derived groups tend to have compact wings (positive PC1 values). Accordingly, variation in wing aspect ratio was strongly structured by phylogeny (Fig. 2B,D), and exhibited the strongest phylogenetic signal among all morphological parameters (K = 0.69; Table S1). PC2 accounted for 12% of the total shape variation, and primarily captured shape changes corresponding to variation in the normalized radius of gyration, r_2^* (Fig. 2C,E). Higher PC2 values indicate greater distal distribution of wing area, while lower values reflect area concentrated near the wing base. This axis of shape variation was allometric, being significantly correlated with body mass (PGLS of PC2 against body mass: R^2=0.16; t=-4.75, p <0.001) (Fig. 2E). Although less clearly associated with phylogeny, r_2^* still exhibited a significant phylogenetic signal (Fig. 2C; K = 0.24; Table S1).

Interestingly, variation in body shape paralleled that of wing shape, as the correlation between wing and body aspect ratio was significant and positive (r=0.69; t=11.12, p <0.001), with more basal groups tending toward elongated high-aspect ratio body and wing forms. Shape characteristics thus mainly differentiated Dipteran taxa, ranging from slender morphologies in basal taxa to stouter bodies in more derived ones. In contrast, body size was markedly more variable within taxa and showed no significant phylogenetic signal (Table S1).

Diversity in hovering flight kinematics and aerodynamics among Diptera

The quantification of hovering flight kinematics effectively captured inter-specific variation, with differences between species mostly larger than individual variability across flight sequence within the same species (Fig. S2 and Table S2).

Overall, the wingbeat kinematics of the 46 Dipteran species were remarkably similar across the phylogeny, with the exception of the two basal groups Culicomorpha (mosquitoes and midges) and Tipulomorpha (crane flies) (Fig. 3, Video S1). Wingbeat frequency and stroke amplitude were conserved within relatively narrow ranges, at $f =$ 236 [201–270] Hz and $A_\phi = 117^\circ$ [110°–124°], respectively (mean [95% confidence interval]; Fig. 3I). In contrast, Culicomorpha and Tipulomorpha showed striking divergence, with mean wingbeat frequencies reaching 714 Hz and 70 Hz, respectively (Fig. 3C).

Focusing on the temporal dynamics of their wingbeat kinematics show similar trends (Fig. 3C–E, Video S1). In all species, the wingbeat involved a forward and backward wing movement following a sinusoidal pattern within the stroke plane (Fig. 3C), with a relatively narrow range in stroke amplitude ($A_\phi = 117^\circ$ [110°–124°]). Culicomorpha are here a clear outlier, with exceptionally low amplitudes ($A_\phi = 37^\circ$ [32°– 42°]). Movements outside the stroke plane, reflected by the deviation angle, were for all Dipteran species minimal (Fig. 3E). As such, the oscillatory angular speed of the wingbeats was primarily caused by the wing stroke movement, with peak of angular speed $\omega = 68^\circ$ [62°–74°] $\times 10^3$ s^{-1} (Fig. 3F). Here, Tipulomorpha were the outlier, with exceptionally low wing stroke speeds ($\omega = 21^\circ$[14°– 27°] $\times 10^3$ s^{-1}), caused by their low wingbeat frequencies. For most wingbeats, the wing maintained a relatively constant rotation angle during the mid forward and backward strokes, often exhibiting a 'double peak' pattern (Fig. 3E). At the end of both the forward and backward strokes, the wings quickly supinated and pronated, respectively. This causes the wing to flip upside down at stroke reversal, allowing it to operate again at a positive constant angle of attack α, required for producing an upward-directed aerodynamic force (Fig. 3G). The angle-of-attack at mid-stroke varied very little across species ($\alpha = 45^\circ$[44°– 47°]).

The conserved wingbeat pattern among most Diptera resulted in similarly conserved aerodynamic force production, as measured by the force coefficients normal and tangential to the wing stroke plane, derived from CFD (Fig. 3G and 3H, respectively). For all Diptera, the temporal dynamics of the normal force coefficient ($C_N(t)$) shows a double peak, one during each wing stroke, resulting in a wingbeat-average net normal force coefficients of $C_N = 1.66$ [1.57–1.74] (Fig. 3G). The temporal dynamics of the tangential force coefficient ($C_T(t)$) is also conserved among most species, generating a peak force at each mid wingstroke (Fig. 3H); here the backstroke peak is negative due to the reversed wing movement. In contrast to the conserved temporal dynamic in $C_N(t)$ in most Diptera, that of $C_T(t)$ was in Culicomorpha species strikingly divergent from the norm. In these species, tangential forces were markedly higher than for other Diptera, which also occured early in the wingbeat. This difference is reflected in the larger wingbeat-average tangential forces for Culicomorpha ($C_T = 4.17$ [3.35–4.99]) than for all Diptera ($C_T = 2.06$ [1.79–2.34]).

Regarding general flight kinematics, the mean flight speed was $U_\infty = 0.76$ [0.71–0.81] m s^{-1}, while the mean body pitch and climb angle were $\beta_{\text{body}} = 31^\circ$ [28°– 34°]) and $\gamma = 20^\circ$ [16°– 25°], respectively. However, these two angles showed greater variability between individuals than between species, obscuring possible species-specific differences. Similarly, the stroke plane angle $\beta_{\text{stroke-plane}} = -15^\circ[-19^\circ - -11^\circ]$ showed higher variability within than between species (see Fig. S2 and Table S2 for inter- vs intra-specific variation in all flight parameters). The mean advance ratio was close to the generally accepted threshold of 0.1 (J=0.13 [0.12–0.14]), showing that the studied Diptera were operating relatively close to a hovering flight mode.

Wingbeat kinematics showed significant phylogenetic signal for all parameters (K-multivariate = 0.01; p = 0.29), excepted for the angle-of-attack that was not influenced by phylogeny (see Fig. S1 for parameter-specific values), suggesting strong aerodynamic constraints limiting its variation.

Allometric adaptations in morphology and wingbeat kinematics for maintaining weight support

We tested how hovering Diptera of different sizes maintain weight support ($2F_V = mg$), through allometric adaptations in wing morphology and wingbeat kinematics (Fig. 4). This revealed that, among the morphological parameters that primarily affect aerodynamic force production (Eqn 3), wingspan (b) and normalized radius of gyration (r_2^*) show negative allometric scaling with body mass (Fig. 4A and 4B, respectively); in contrast, aspect ratio (AR) did not scale with size (Fig. 4C). Thus, tiny Diptera species have relatively larger wingspans than larger species, and have more spatulated wings (high r_2^*). Both mechanisms allow tiny fliers to (partly) compensate for the reduction in aerodynamic force production under isometric scaling. While aspect ratio did not scale with size, it varied primarily with phylogeny (Fig. 2), with Culicomorpha and Tipulomorpha having exceptionally high aspect ratio wings (Fig. 4C; among all Diptera: AR=3.86 [3.72–4.00]; among Culicomorpha and Tipulomorpha: AR=5.23 [4.93–5.54].

Among the wingbeat kinematics parameters that affect aerodynamic force production (Eqn 3), both wingbeat frequency and angle-of-attack exhibited negative allometric scaling with body mass (Fig. 4D and 4F, respectively); wingstroke amplitude did not scale with size (Fig. 4E). Thus, tiny Dipteran fliers beat their wings at high wingbeat frequencies than larger species, and do so at higher wingbeat-average angles-of-attack; in contrast, they do not significantly increase their wingstroke amplitude. The increase in wingbeat frequency allow tiny fliers to almost fully compensate for the reduction in aerodynamic force production under isometric scaling (Fig. 4D). In contrast, the increase in angle-of-attack for tiny Diptera seems to cause a corresponding reduction in the vertical force coefficient, which show a positive allometric scaling with size (Fig 4G). This is expected because the angles-of-attack in tiny flyers are higher than 45° (Phan and Park, 2018). In this scaling analysis, Culicomorpha and Tipulomorpha are again outliers with strikingly high and low wingbeat frequencies for their size, respectively (Fig. 4C; all Diptera: f=236 [201 –270] Hz; Culicomorpha: f=715 [615–814] Hz; Tipulomorpha: f=70 [51–89] Hz). Hovering Culicomorpha have also strikingly low wingstroke amplitudes (Fig. 4E; all Diptera: A_ϕ=117° [110°–124°]; Culicomorpha: A_ϕ=37° [32°–42°]).

These combined results suggest that allometric adaptations in both morphology and wingbeat kinematics allow Diptera of different sizes to maintain weight support during hovering flight. We estimated the relative contribution of allometric adaptations in the different morphology and kinematics parameters to maintain weight support across sizes, by calculating the relative allometric scaling factor a^* (Fig. 4H). This showed that allometric adaptations in wingbeat frequency contributed the most to maintain weight support across sizes (61%), followed by wingspan (43%). Allometric adaptations in normalized radius of gyration contributed relatively little (3%), whereas the scaling in vertical force coefficient had a detrimental negative effect (-8%).

Scaling of aerodynamic power with size and phylogeny

In addition to maintaining weight support, flying Diptera are expected to minimize the power required for flight. We combined CFD with physical scaling law models (Eqn. 5) to assess how aerodynamic power in hovering flight scales with size, phylogeny, kinematics and aerodynamics (Fig. 5). The weight-normalized aerodynamic power (P^*_{aero}) scales positively with body mass (PGLS regression: R^2=0.18; p=0.003). This effect is strongest for the relatively large Diptera, and seems to even inverse for the smallest ones. Moreover, Culicomorpha and Tipulomorpha seem

outliers, with a relatively high and low aerodynamic power requirement, respectively. The resulting observed slope of the PGLS regression (a=0.07 [0.02 –0.12]) was significantly lower than that expected under morphological and kinematic similarity (a_{sim}=0.17), confirming that smaller Diptera exhibit disproportionately higher power demands relative to their body mass.

According to our model (Eqn. 5), the weight-normalized aerodynamic power scales with the product of wing speed and relative drag ($P^*_{\text{aero}} = U_D\, D^*$). We first tested the validity of this model by comparing the model-predicted power with those estimated from CFD. These two metrics were highly correlated (coefficient of correlation r = 0.92; p< 0.001), showing that our simplified aerodynamic power model predicts energy expenditure based on morphology and wingbeat kinematics well. Second, we used the model to separate the effects of kinematics (U_D) and aerodynamics (D^*) on the power requirement for flight (Fig. 5A-C).

According to the PGLS regression, wing speed (U_D) scaled positively with body mass as $U_D \sim m^{0.16\ [0.13\text{–}0.19]}$ (Fig. 5B, Table 1). This scaling is significantly lower than expected under morphological and kinematic similarity ($a_{\text{sim}} = 0.33$), but closely aligns with the theoretical scaling required for weight support ($a_{\text{ws}} = 0.17$). Moreover, wing speed during hovering flight seems highly conserved among Diptera, including Culicomorpha with their high-frequency low-amplitude wingbeats ($U \sim f\ A$). The flapping wings of Tipulomorpha seem to operate at relatively low speeds, for their respective size.

In contrast with wing speed, the wingbeat-average relative drag seem to decrease with increasing size, at least for small Diptera (Fig. 5C). In fact, among the largest Diptera relative drag seems to be relatively conserved at $D^* \sim 1.25$. Also, here Culicomorpha are outliers, with exceptionally high drag.

The negative correlation between relative drag and body mass could be explained by the effect of Reynolds number on (viscous) drag on an airfoil. We tested this by comparing our CFD-based drag estimates with the classic scaling of drag with Reynolds number (Ellington, 1984b; Lyu et al., 2019)(Fig. 5F). This shows that these Re-based scaling align surprisingly well with the wingbeat-average relative drag in hovering Diptera: At Re>300 the relative drag remains rather constant at $D^* \approx 1.25$; in contrast, at Re<300 relative drag increases with decreasing Reynolds number as $D^* \approx 24/\sqrt{\text{Re}}$. Because Reynolds number scales with body mass as $\text{Re} \sim \sqrt{m}$, similar scaling is found between relative drag and body mass ($D^* \approx 1.25$; and $D^* \approx 24\ m^{1/4}$ (Fig. 6C). Thus, for large Dipera ($m > 2$ mg), relative drag remains approximately constant, whereas for small Diptera ($m < 2$ mg) drag increases with decreasing body mass, due to a Re-dependent increasing in viscous drag. Here, Culicomorpha are again outliers, due to their exceptionally high relative drag, for both their size and the Reynolds number their operate at during hovering flight.

The wingbeat-average relative drag equals the ratio between the drag coefficient and vertical force coefficient ($D^* = C_D/C_V$). The temporal dynamics of both coefficients reveal the underlying cause of the elevated drag in Culicomorpha (Fig. 6D-E). The temporal dynamics of both C_D and C_V are highly conserved among most Diptera, but not for Culicomorpha. Here especially the drag coefficient values are exceptionally high, mostly at the start of each wing stroke, and thus the relative drag seems relatively high for hovering Culicomorpha primarily due to the increase in the corresponding drag coefficient (not a decrease in C_V).

The combined scaling of wing speed (U_D) and relative drag (D^*) with body mass (Fig. 5B-C) helps explain the scaling of the normalized power with body weight (Fig. 5A). For large Diptera ($m > 2$ mg) the combination of constant D^* with positive scaling of wing speed, results in a positive scaling of normalized aerodynamic power with mass as $P^*_{\text{aero}} \sim m^{1/6}$. For small Diptera ($m < 2$ mg), the positive and negative scaling of wing speed and relative drag, respectively, partly cancel each other, resulting in a relatively weak scaling of aerodynamic power with mass as $P^*_{\text{aero}} \sim m^{-1/12}$. This might be true for both Culicomorpha and other tiny Diptera, but with a drag penalty

in mosquitoes and midges due to their high-frequency wingbeat. In contrast, Tipulomorpha exhibited the lowest aerodynamic power relative to their body size, due to their low-speed wingbeats, as the relative drag on their wings are on par with other Diptera.

Scaling of acoustic power with size and phylogeny

We continued to test whether and how the high-power wingbeat of mosquitoes and midges produce increased aero-acoustic sound, potentially driven by sexual communication. For this, we estimated the far-field sound produced by the beating wings by augmenting our CFD results with aero-acoustic modeling (Fig. 6). This shows that sound power scales positively with body mass as $P_{\text{acoustic}} \sim m^{1.57[1.38–1.76]}$ (PGLS regression: R^2=0.86; $p < 0.001$; Fig. 6A). This scaling is not significantly different from the expected scaling for maintaining weight support under isometric conditions ($P_{\text{acoustic}} \sim m^{5/3}$; see supplementary text for details). These results show that, for Diptera in general, there seem no allometric adaptations present for sound production. In contrast, this is clearly different for the infraorder Culicomorpha, who exhibited disproportionately high sound power levels relative to their body mass (Fig. 6A).

Secondly, we estimated the dimensional aero-acoustic power (P^*_{acoustic}), from CFD, kinematics and morphology (Eqn. 9), and tested how scales with relative drag D^* (Fig. 6B). This resulting PGLS regression was positive, indicating a trade-off between acoustic and aerodynamic performance. Striking is that here the data for Culicomorpha were not trend-breaking, but that for these insects both acoustic power and relative aerodynamic where enhanced relative to other Diptera. This shows that Culicomorpha primarily produce enhanced acoustic power by producing increased relative aerodynamic drag.

Scaling of muscle and aerodynamic power with size and phylogeny

The aerodynamic power required for flight is produced by the flight muscles. To test for adaptations in this musculature, we compared aerodynamic power with relative muscle mass and the expected power output of these muscles (Fig. 7).

The available relative muscle mass did not show a significant scaling with body mass in all Diptera (PGLS regression: $R^2 = 0.12$; $p = 0.193$), largely due to the Culicomorpha species possessing a markedly higher relative muscle mass than other taxa (Fig. 1C and 7B). However, when Culicomorpha were excluded, the relative muscle mass increased significantly with body mass, increasing with mass to the power of a = 0.08 [0.06 –0.11] (PGLS regression: $R^2 = 0.85$; $p < 0.001$). This exponent deviates significantly from the isometric expectation of a_{sim}=0, but remains below the mass-specific scaling of the relative aerodynamic power for large Diptera ($a = 0.17$; Fig. 7A).

That said, the direct comparison between required aerodynamic power and available muscle power (Fig. 7A and 7B, respectively) shows strong similarities. Among large Diptera both powers scale positively with body mass, which reduces or even reverses in tiny Diptera. Moreover, Culicomorpha have both increased required and available power, for their relative small size. Directly comparing the required and available power across species where both measures were obtained shows that Diptera consistently possess approximately twice the power required for flight. These dynamics include all Diptera including the energetically highly inefficient Culicomorpha and efficient Tipulidae.

DISCUSSION

Here, we present one of the most comprehensive comparative biomechanical studies of insect flight within a phylogenetic framework, investigating the factors influencing flight diversity in Diptera, one of the largest and most ecologically diverse insect orders (Wiegmann and Yeates, 2017; Grimaldi and Engel, 2005; Yeates and Wiegmann, 2005). We quantified wingbeat kinematics, morphological traits, and aerodynamic and acoustic efficiency across the phylogeny, thereby revealing how biomechanical traits diversifies across Diptera. By evaluating the extent to which the observed diversity in these traits can be explained by physical scaling laws and aerodynamic principles, we also highlight deviations that likely reflect adaptive responses to selective pressures.

Conserved and divergent traits in Diptera flight motors system

Despite the wide ecological diversity of Diptera and its potential influence on trait evolution, our results show that wingbeat kinematics is relatively well conserved across their phylogeny. Even among highly divergent lineages, flight is achieved through remarkably similar wingbeat kinematics, with conserved temporal dynamic of wing stroke, deviation, and rotation angles. This demonstrates the dominant role of aerodynamic constraints in shaping the evolution of flight. The persistence of such a broadly consistent flapping-wing propulsion system across diverse Dipteran taxa, and potentially more generally across insects and even other flapping-flying animals (Chin and Lentink, 2016), suggests that it may have been key to their ability to exploit a wide range of ecological niches. Two notable exceptions stood out from this general pattern: species from the infraorders Culicomorpha (mosquitoes and midges) and Tipulomorpha (crane flies). In Culicomorpha, wingbeat frequency was exceptionally high and stroke amplitude markedly reduced compared to other Diptera. Conversely, Tipulomorpha species exhibited markedly low wingbeat frequencies relative to all other taxa. This suggests that flight in these two groups may have been shaped by distinct selective regimes compared to more recently diverged taxa.

Variation in wingbeat kinematic was nonetheless affected by the phylogeny. Indeed, we detected a significant phylogenetic signal in most wingbeat kinematic parameters, except for wing angle-of-attack, which showed very limited interspecific variation and thus appears to be the most tightly constrained by aerodynamic requirements.

In comparison with wingbeat kinematics, variation in wing and body morphology across species was more structured by phylogeny. This finding challenges the general view that behavioral traits are more evolutionarily labile than morphological traits (Blomberg et al., 2003), and further emphasizes that Diptera have evolved highly specialized wingbeat kinematics, conserved across morphologically distinct species.

Our results show that morphological shape (including wing and body aspect ratio) primarily distinguishes Dipteran taxa, with most basal lineages exhibiting elongated high aspect-ratio forms and derived ones showing stouter low aspect-ratio morphologies. Whether evolutionary changes in wing and body shape across Diptera are primarily adaptive or stem from neutral evolutionary processes is challenging to ascertain. Early-diverging Diptera may have retained morphologies closer to the ancestral state (slender body, high aspect-ratio wings), while the diversification of subsequent lineages into varied ecological niches may have promoted the evolution of stouter wing and body shape. Such morphology reduces the moment of inertia, allowing faster rotations and overall enhancing maneuverability – a key component of flight performance under strong selection for tasks such as capturing prey, evading predators, or navigating cluttered environments (Crall et al., 2015; Wardill et al., 2017; Srygley and Dudley, 1993). This advantage, however, may come at the cost of increased energetic demands. A possible interpretation to the observed morphological pattern is that selective pressures favoring enhanced maneuverability were less pronounced in early Diptera.

Assessing the adaptive significance of these trait changes is particularly difficult at the order-wide scale of our study. Indeed, adaptive divergence is more readily inferred when comparing closely related species with contrasting ecologies (e.g., Skowron Volponi et al., 2018; Aiello et al., 2021b; Le Roy et al., 2021), where phylogenetic inertia and unknown selective pressures play a smaller role. While our macroevolutionary analysis reveals broad patterns, finer-scale comparative work is needed to disentangle neutral divergence from ecological adaptation.

In contrast with morphological shape, body size was more variable within taxa, suggesting that size might be less phylogenetically constrained than shape in Diptera. Body size, however, imposes strong physical and aerodynamic constraints on flight-related traits.

Scaling and aerodynamic constraints structure Diptera flight diversity

Much of the variation in animal morphological and biomechanical traits can generally be explained by scaling laws, i.e., how traits change with body size (Gould, 1966; Pélabon et al., 2014; Cloyed et al., 2021). In flying animals, an additional key constraint is the need to generate sufficient lift to support body weight, which strongly affect the evolution of morphological and biomechanical traits (Norberg, 2007; Dudley, 2002).

Weight support requirement in hovering flight

Our analysis of the scaling relationships between body mass and flight-related traits demonstrates the strong influence of physical scaling laws and aerodynamic constraints. When size decreases isometrically, the wings become relatively less effective in producing the aerodynamic forces required for weight support, which may promote the evolution of disproportionately large wings in smaller species, or a compensatory change in wingbeat kinematics (e.g., increased wingbeat frequency or amplitude). In line with these predictions, we observed relatively larger wings in smaller species than expected under isometry (geometric similarity). Wing shape also scaled allometrically with size: the normalized radius of gyration was slightly higher in smaller species, indicating a shift in wing area distribution more distally, which enhances aerodynamic force production (Muijres et al., 2017b). Wingbeat kinematics likewise varied with size, with both wingbeat frequency and angle-of-attack increasing as body size decreased. Here, the increase in wingbeat frequency had a compensatory effect to the reduction in relative lift force production with decreasing size, whereas the corresponding increase in angle-of-attack was detrimental, due to a reduction in the vertical force coefficient. In contrast with wingbeat frequency and angle-of-attack, wing stroke amplitude was relatively constant across sizes in the studied Diptera. Altogether, the combined allometric adaptations in both morphology and wingbeat kinematics lead to a relative increase in lift production with decreasing size, compensating for the reduction in weight support associated with isometric size reduction.

Assessing the relative contributions of allometric adaptations of the different traits to weight support highlighted that increases in wingbeat frequency and relatively larger wingspan were the dominant compensatory mechanisms, accounting for 61% and 43% of all allometric adaptations combined, respectively. In comparison, changes in the normalized radius of gyration has a minor 3% contribution, whereas the angle-of-attack induced changes in vertical force coefficient has a detrimental effect of -8%.

Our scaling analysis thus shows that Diptera primarily rely on kinematic adjustments to maintain weight support across size, consistent with patterns reported in other flying animals (Dudley, 1990; Darveau et al., 2005; Tercel et al., 2018; Norberg, 2007; Rayner, 1988; Riskin et al., 2010). This finding, however, contrasts with results obtained in some studies performed at smaller phylogenetic scale. For instance, scaling analysis in hoverflies (Le Roy et al., 2025; Belyaev et al., 2014), bees (Duell et al., 2022; Grula et al., 2021) or sphingid moths (Bartholomew and Casey, 1978) show that morphological adjustments across size dominate over kinematic changes. These results suggest

that, at large evolutionary scales, kinematics flexibility might primarily allow maintaining weight support because morphology is more constrained by phylogeny (Blomberg et al., 2003). Conversely, at smaller phylogenetic scales, the contribution of morphological adjustments to maintaining weight support across size may be more apparent.

Power requirement for hovering flight in Diptera

Computational Fluid Dynamic (CFD) simulations revealed that aerodynamic power scales predictably with body size, in line with theoretical expectations. Specifically, among large Dipteran fliers, weight-normalized aerodynamic power scaled positively with size due to the positive isometric scaling of wing speed with size ($U_D \sim m^{1/6}$). In contrast, in tiny Diptera ($m < 2$ mg), the weight-normalized aerodynamic power plateaued, and even slightly increase with decreasing size. This effect corresponds to a drop in aerodynamic efficiency at low Reynolds numbers ($\mathrm{Re} < 400$), where viscous forces become increasingly dominant. In this regime, drag rises disproportionately relative to lift (Ellington, 1984b; Lyu et al., 2019).

Thus, as body mass decreases beyond 2 mg, the aerodynamic power remains relatively stable due to two compensatory effects: a decrease in power due to positive isometric scaling of wing speed, and a negative scaling due to elevated relative (viscous) drag at lower Reynolds number. For the tiniest fliers that operate in the viscous Reynolds number regime, the increased viscous drag likely exerts a strong constraint on the evolution miniaturized flying insects (Polilov, 2015; Farisenkov et al., 2022).

The scaling of available power for flight, inferred from thorax mass, closely matched the scaling of aerodynamic power requirements from CFD simulations, underscoring the tight co-evolution of muscle morphology and aerodynamic demands (Ellington, 1984b; Lyu and Sun, 2021). This alignment ensures that power supply and demand remain balanced, avoiding performance failure or metabolic inefficiency (Dudley, 2002; Norberg, 1996). We show that most Diptera maintain a two-fold safety margin, consistent with previous findings (Gilmour and Ellington, 1993; Lehmann and Dickinson, 1997). This excess muscle capacity likely safeguards performance under demands for maneuverability or environmental variability (e.g., windy condition or predator attack). This even includes Culicomorpha and Tipulomorpha species, in which we observed a combination of increased and reduced power requirements and flight musculature, respectively. The increased musculature enables Culicomorpha to fly with their exceptionally costly high-frequency wingbeats, and for females to carry large blood-loads after feeding (Muijres et al., 2017a). These results highlight how physical constraints, energetic optimization, and lineage-specific selective pressures jointly shape the evolution of the Diptera flight motor system.

The observed scaling between aerodynamic power requirements, available motor power, and body mass provides a baseline around which most Diptera species cluster. Deviations from this trend may point at evolutionary trade-offs. While insufficient aerodynamic power risks flight failure, excessive investment in increased flight power musculature may reflect selective pressures favoring specialized flight performance. For example, higher power demands may be under selection in predatory species where rapid acceleration is crucial for prey capture (e.g., in robber flies, Wardill et al., 2017), or in species where prolonged period of hovering flight increase mating success (e.g., in hoverflies, Gilbert, 1984; Le Roy et al., 2025). By contrast, in species with lifestyles that place little demand on maneuverability, selection may favor reduced flight costs, as observed here in Tipulomorpha, where exceptionally low energetic demands may have evolved at the expense of maneuverability. Strikingly, our results reveal a major departure from the general scaling pattern in a subset of the smallest species. Culicomorpha (mosquitoes and midges) exhibited power requirements nearly three times higher than other taxa of comparable size. This elevated flight cost stems from the exceptionally high wingbeat frequency observed in these species, and is associated with larger relative

thoracic muscle mass providing greater available power for flight.

Trade-off between aerodynamic and acoustic efficiency in mosquitoes and midges

The flight of mosquitoes has been extensively studied in the context of sound production and its role in locating sexual partners (Wishart and Riordan, 1959; Belton, 1994; Gibson and Russell, 2006; Cator et al., 2009; Seo et al., 2019). It has been shown that male and female mosquitoes adjust their flight tones during swarming, enabling acoustic mate recognition (Pennetier et al., 2010). Selection for effective acoustic signaling, essential for mosquito reproduction, may thus come at the expense of flight cost minimization. Consistent with the hypothesis that sexual communication imposes strong selective pressures on mosquito flight, our comparative analysis highlight the strong divergence of muscular morphology and wingbeat kinematics between Culicomorpha and all other studied Diptera. Moreover, we showed that mosquitoes and midges produce substantially higher acoustic power for their size compared to other Diptera, which they achieve by simultaneously increasing their wingbeat frequency and reducing their wingstroke amplitude. These adaptations in wingbeat kinematics come at the expense of an increase in aerodynamic power requirement for hovering flight, and a corresponding increase in flight motor musculature. Selection for effective acoustic communication has thus strongly affected the evolution of biomechanical traits in Culicomorpha, highlighting a evolutionary compromise, where reproductive success prevail over aerodynamic efficiency.

Conclusion

Our comparative study on Diptera flight highlights how the interplay between physical scaling laws, aerodynamic constraints, and both ecological and sexual selection shapes the evolution of complex locomotor systems. Beyond Diptera, our results provide a mechanistic framework for understanding how biomechanical and evolutionary forces interact to generate diversity in animal flight, offering insights relevant to evolutionary biology, functional morphology, and bio-inspired engineering.

LIST OF SYMBOLS AND ABBREVIATIONS

a	scaling factor of a metric with body mass ($\sim m^a$)	[-]
a^*	relative scaling factor of a metric with body mass	[-]
A_ϕ	wingstroke amplitude	[°]
α	wing angle-of-attack	[°]
AR	wing aspect ratio (b^2/S)	[-]
b	wingspan	[m]
$\bar{c}$	mean wing chord (S/b)	[m]
c_s	speed of sound in air	[m s^{-1}]
C_D	drag coefficient	[-]
C_F	aerodynamic force coefficient	[-]
C_L	lift coefficient	[-]
C_p	pressure coefficient	[-]
C_V	vertical force coefficient	[-]
C_H	horizontal force coefficient	[-]

C_N	stroke-plane normal force coefficient	[-]
C_T	stroke-plane tangential force coefficient	[-]
C_{var}	coefficient of variation	[%]
CFD	Computational Fluid Dynamics	
D	drag force	[N]
D^*	weight-normalized relative drag force	[-]
DLT	Direct Linear Transformation	
η	wing deviation angle (out of stroke-plane)	[°]
f	wingbeat frequency	[Hz]
F	aerodynamic force	[N]
F_p	pressure force	[N]
F_V	vertical force	[N]
F_H	horizontal force	[N]
g	gravitational acceleration	[m s^{-2}]
γ_{climb}	climb angle	[°]
J	advance ratio	[-]
K	Blomberg's K-statistic (phylogenetic signal)	
L	lift force	[N]
m	body mass	[kg]
m_{dry}	dry body mass	[kg]
m_{muscle}	flight muscle mass	[kg]
Ω	angular velocity vector	[rad s^{-1}]
ω	angular speed of wing	[rad s^{-1}]
p'	pressure fluctuation	[Pa]
P_{aero}	aerodynamic power	[W]
P^*_{aero}	weight-normalized aerodynamic power	[W kg^{-1}]
P_{acoustic}	acoustic power	[W]
P^*_{acoustic}	Non-dimensional acoustic power	[W kg^{-2}]
$P_{\text{available}}$	available power from muscles	[W]
P^*_{muscle}	mass-specific muscle power output	[W kg^{-1}]
PC	Principal Component	
PCA	Principal Component Analysis	
PGLS	Phylogenetic Generalized Least Squares	
p	probability value	
ϕ	wing stroke angle (within stroke-plane)	[°]
ψ	body yaw angle	[°]
q	dynamic pressure	[Pa]
r	radial distance from sound source	[m]
r_2	radius of gyration of wing	[m]
r_2^*	span-normalized radius of gyration (r_2/b)	[-]
r_D^*	span-normalized moment arm of drag force	[-]

Re	Reynolds number	[-]
r	correlation coefficient	
R^2	coefficient of determination	
ρ	air density	[kg m^{-3}]
S	wing surface area	[m^2]
S_2	wing second-moment-of-area relative to hinge	[m^4]
t	time	[s]
t'	retention time	[s]
t^*	wingbeat cycle period (tf)	[-]
T_{aero}	aerodynamic torque	[N m]
t	regression	
θ	wing rotation angle (along spanwise axis)	[°]
U	flight speed	[m s^{-1}]
U_D	average wing speed at drag force moment arm	[m s^{-1}]
U_{hor}	horizontal flight velocity component	[m s^{-1}]
U_r	wingbeat-average wing speed	[m s^{-1}]
U_{ver}	vertical flight velocity component	[m s^{-1}]
υ	kinematic viscosity of air	[m^2 s^{-1}]
φ	body roll angle	[°]
WABBIT	Wavelet Adaptive Block-Based solver for Insects in Turbulence	
$\mathbf{X} = [x, y, z]$	coordinates in the world reference frame, with the z axis vertical up	[m]
β_{body}	body pitch angle	[°]
$\beta_{\text{stroke-plane}}$	stroke-plane pitch angle	[°]

ACKNOWLEDGMENTS

The authors gratefully acknowledge the late Paul Beuk, whose enthusiasm and knowledge of Diptera taxonomy left a lasting impression and provided valuable context for this work. We thank Antoine Cribellier, Guillermo Amador, and Abel-John Buchner for helpful discussions on the quantification of insect flight. We are grateful to Remco Pieters for his assistance in building and operating the experimental setup, and to Henk Schipper and Michel Breuer for their support with laboratory work. We thank Serge Poda and Tessa Visser for providing the lab-reared Diptera specimens, and Uroš Cerkvenik for his help in determining relative muscle data of large horseflies.

FUNDINGS

This work was supported by an NWO Vidi research grant to F.T.M. (I/VI.Vidi.193.054), and by computational and storage resources provided to T.E. by GENCI at IDRIS and TGCC (2025-A0182A14152). Resources were allocated on the Jean Zay supercomputer (CSL partition), and on the Skylake and Rome partitions of the IRENE supercomputer.

DATA AVAILABILITY STATEMENT

All data underlying the findings of this study are fully available without restriction. The morphological, kinematics and aerodynamics data, microscope images and high-speed videos for all studied species are deposited in the Dryad

Digital Repository under DOI: 10.5061/dryad.gxd25480s (temporary Dryad reviewer link). DNA barcode data for all analyzed specimens are publicly available in the BOLD System project DIPTR via this link. No ethical or legal restrictions apply to the sharing of these data.

REFERENCES

Adams, D. C. (2014). A generalized k statistic for estimating phylogenetic signal from shape and other high-dimensional multivariate data. *Systematic biology*, 63(5):685–697.

Adams, D. C., Rohlf, F. J., and Slice, D. E. (2004). Geometric morphometrics: ten years of progress following the 'revolution'. *Italian Journal of Zoology*, 71(1):5–16.

Agrawal, S., Grimaldi, D., and Fox, J. L. (2017). Haltere morphology and campaniform sensilla arrangement across diptera. *Arthropod Structure & Development*, 46(2):215–229.

Aiello, B. R., Sikandar, U. B., Minoguchi, H., Bhinderwala, B., Hamilton, C. A., Kawahara, A. Y., and Sponberg, S. (2021a). The evolution of two distinct strategies of moth flight. *Journal of the Royal Society Interface*, 18(185):20210632.

Aiello, B. R., Tan, M., Bin Sikandar, U., Alvey, A. J., Bhinderwala, B., Kimball, K. C., Barber, J. R., Hamilton, C. A., Kawahara, A. Y., and Sponberg, S. (2021b). Adaptive shifts underlie the divergence in wing morphology in bombycoid moths. *Proceedings of the Royal Society B*, 288(1956):20210677.

Alexander, R. M. (2003). *Principles of animal locomotion*. Princeton university press.

Baliga, V., Szabo, I., and Altshuler, D. (2019). Range of motion in the avian wing is strongly associated with flight behavior and body mass. *Science advances*, 5(10):eaaw6670.

Barenblatt, G. I. (2003). *Scaling*, volume 34. Cambridge University Press.

Bartholomew, G. A. and Casey, T. M. (1978). Oxygen consumption of moths during rest, pre-flight warm-up, and flight in relation to body size and wing morphology. *Journal of Experimental Biology*, 76(1):11–25.

Belton, P. (1994). Attractton of male mosquitoes to sound. *J Am Mosq Control Assoc*, 10:297–301.

Belyaev, O., Chukanov, V., and Farisenkov, S. (2014). Comparative characteristics of the wing apparatus and flight of syrphid flies (diptera: Syrphidae). *Moscow University biological sciences bulletin*, 69:19–22.

Blomberg, S. P., Garland Jr, T., and Ives, A. R. (2003). Testing for phylogenetic signal in comparative data: behavioral traits are more labile. *Evolution*, 57(4):717–745.

Bomphrey, R. J., Nakata, T., Phillips, N., and Walker, S. M. (2017). Smart wing rotation and trailing-edge vortices enable high frequency mosquito flight. *Nature*, 544(7648):92–95.

Bookstein, F. L. (1997). *Morphometric tools for landmark data*.

Broadley, P. and Nabawy, M. R. (2022). An experimental investigation of reynolds number effects on the aerodynamics of insect-like revolving wings. In *AIAA SCITECH 2022 Forum*, page 0307.

Buchwald, R. and Dudley, R. (2010). Limits to vertical force and power production in bumblebees (hymenoptera: Bombus impatiens). *Journal of experimental Biology*, 213(3):426–432.

Byrne, D. N., Buchmann, S. L., and Spangler, H. G. (1988). Relationship between wing loading, wingbeat frequency and body mass in homopterous insects. *Journal of Experimental Biology*, 135(1):9–23.

Cator, L. J., Arthur, B. J., Harrington, L. C., and Hoy, R. R. (2009). Harmonic convergence in the love songs of the dengue vector mosquito. *Science*, 323(5917):1077–1079.

Chapman, J. W., Reynolds, D. R., and Wilson, K. (2015). Long-range seasonal migration in insects: mechanisms, evolutionary drivers and ecological consequences. *Ecology letters*, 18(3):287–302.

Cheng, B., Deng, X., and Hedrick, T. L. (2011). The mechanics and control of pitching manoeuvres in a freely flying hawkmoth (manduca sexta). *Journal of Experimental Biology*, 214(24):4092–4106.

Chin, D. D. and Lentink, D. (2016). Flapping wing aerodynamics: from insects to vertebrates. *Journal of Experimental Biology*, 219(7):920–932.

Cloyed, C. S., Grady, J. M., Savage, V. M., Uyeda, J. C., and Dell, A. I. (2021). The allometry of locomotion. *Ecology*, 102(7):e03369.

Combes, S., Rundle, D., Iwasaki, J., and Crall, J. D. (2012). Linking biomechanics and ecology through predator–prey interactions: flight performance of dragonflies and their prey. *Journal of Experimental Biology*, 215(6):903–913.

Crall, J. D., Ravi, S., Mountcastle, A. M., and Combes, S. A. (2015). Bumblebee flight performance in cluttered environments: effects of obstacle orientation, body size and acceleration. *Journal of Experimental Biology*, 218(17):2728–2737.

Cribellier, A., Camilo, L. H., Goyal, P., and Muijres, F. T. (2024). Mosquitoes escape looming threats by actively flying with the bow wave induced by the attacker. *Current Biology*, 34(6):1194–1205.

Cribellier, A., Straw, A. D., Spitzen, J., Pieters, R. P., van Leeuwen, J. L., and Muijres, F. T. (2022). Diurnal and nocturnal mosquitoes escape looming threats using distinct flight strategies. *Current Biology*, 32(6):1232–1246.

Danks, H. and Oliver, D. (1972). Seasonal emergence of some high arctic chironomidae (diptera). *The Canadian Entomologist*, 104(5):661–686.

Darveau, C.-A., Hochachka, P. W., Welch Jr, K. C., Roubik, D. W., and Suarez, R. K. (2005). Allometric scaling of flight energetics in panamanian orchid bees: a comparative phylogenetic approach. *Journal of Experimental Biology*, 208(18):3581–3591.

Deora, T., Gundiah, N., and Sane, S. P. (2017). Mechanics of the thorax in flies. *Journal of Experimental Biology*, 220(8):1382–1395.

Deora, T., Singh, A. K., and Sane, S. P. (2015). Biomechanical basis of wing and haltere coordination in flies. *Proceedings of the National Academy of Sciences*, 112(5):1481–1486.

Downes, J. (1969). The swarming and mating flight of diptera. *Annual review of entomology*, 14(1):271–298.

Dudley, R. (1990). Biomechanics of flight in neotropical butterflies: morphometries and kinematics. *Journal of experimental biology*, 150(1):37–53.

Dudley, R. (2002). *The biomechanics of insect flight: form, function, evolution*. Princeton University Press.

Duell, M. E., Klok, C. J., Roubik, D. W., and Harrison, J. F. (2022). Size-dependent scaling of stingless bee flight metabolism reveals an energetic benefit to small body size. *Integrative and Comparative Biology*, 62(5):1429–1438.

Ellington, C. (1984a). The aerodynamics of hovering insect flight. iii. kinematics. *Philosophical Transactions of the Royal Society of London B: Biological Sciences*, 305(1122):41–78.

Ellington, C. (1984b). The aerodynamics of hovering insect flight. iv. aeorodynamic mechanisms. *Philosophical Transactions of the Royal Society of London B: Biological Sciences*, 305(1122):79–113.

Ellington, C. P. (1984c). The aerodynamics of flapping animal flight. *American Zoologist*, 24(1):95–105.

Engels, T., Schneider, K., Reiss, J., and Farge, M. (2021). A wavelet-adaptive method for multiscale simulation of turbulent flows in flying insects. *Commun. Comput. Phys*, 30:1118–1149.

Engels, T., Truong, H., Farge, M., Kolomenskiy, D., and Schneider, K. (2022). Computational aerodynamics of insect flight using volume penalization. *Comptes Rendus. Mécanique*.

Ennos, A. R. (1989). The kinematics and aerodynamics of the free flight of some diptera. *Journal of Experimental*

Biology, 142(1):49–85.

Farisenkov, S. E., Kolomenskiy, D., Petrov, P. N., Engels, T., Lapina, N. A., Lehmann, F.-O., Onishi, R., Liu, H., and Polilov, A. A. (2022). Novel flight style and light wings boost flight performance of tiny beetles. *Nature*, 602(7895):96–100.

Ffowcs Williams, J. E. and Hawkings, D. L. (1969). Sound generation by turbulence and surfaces in arbitrary motion. *Philosophical Transactions of the Royal Society of London. Series A, Mathematical and Physical Sciences*, 264(1151):321–342.

Fontaine, E. I., Zabala, F., Dickinson, M. H., and Burdick, J. W. (2009). Wing and body motion during flight initiation in drosophila revealed by automated visual tracking. *Journal of Experimental Biology*, 212(9):1307–1323.

Fry, S. N., Sayaman, R., and Dickinson, M. H. (2003). The aerodynamics of free-flight maneuvers in drosophila. *Science*, 300(5618):495–498.

Gao, F. and Han, L. (2012). Implementing the nelder-mead simplex algorithm with adaptive parameters. *Computational Optimization and Applications*, 51(1):259–277.

Gibson, G. and Russell, I. (2006). Flying in tune: sexual recognition in mosquitoes. *Current Biology*, 16(13):1311–1316.

Gilbert, F. S. (1984). Thermoregulation and the structure of swarms in syrphus ribesii (syrphidae). *Oikos*, pages 249–255.

Gilmour, K. and Ellington, C. (1993). Power output of glycerinated bumblebee flight muscle. *Journal of experimental biology*, 183(1):77–100.

Gould, S. J. (1966). Allometry and size in ontogeny and phylogeny. *Biological reviews*, 41(4):587–638.

Grimaldi, D. and Engel, M. S. (2005). *Evolution of the Insects*. Cambridge University Press.

Grula, C. C., Rinehart, J. P., Greenlee, K. J., and Bowsher, J. H. (2021). Body size allometry impacts flight-related morphology and metabolic rates in the solitary bee megachile rotundata. *Journal of Insect Physiology*, 133:104275.

Gunz, P. and Mitteroecker, P. (2013). Semilandmarks: a method for quantifying curves and surfaces. *Hystrix, the Italian Journal of Mammalogy*, 24(1):103–109.

Gupta, S., Cribellier, A., Poda, S. B., Roux, O., Muijres, F. T., and Riffell, J. A. (2024). Mosquitoes integrate visual and acoustic cues to mediate conspecific interactions in swarms. *Current Biology*, 34(18):4091–4103.

Hartley, R. I. and Sturm, P. (1995). Triangulation. In *International Conference on Computer Analysis of Images and Patterns*, pages 190–197. Springer.

Hirschberg, A. and Rienstra, S. W. (2004). An introduction to aeroacoustics. *Eindhoven university of technology*, 31.

Hoerner, S. F. (1965). *Fluid-Dynamic Drag: Practical Information on Aerodynamic Drag and Hydrodynamic Resistance*. Hoerner Fluid Dynamics, Brick Town, NJ, USA, 2nd edition. Revised and expanded edition.

Jantzen, B. and Eisner, T. (2008). Hindwings are unnecessary for flight but essential for execution of normal evasive flight in lepidoptera. *Proceedings of the National Academy of Sciences*, 105(43):16636–16640.

Josephson, R. K., Malamud, J. G., and Stokes, D. R. (2000). Power output by an asynchronous flight muscle from a beetle. *Journal of Experimental Biology*, 203(17):2667–2689.

Kirk-Spriggs, A. H. and Sinclair, B. J. (2017). *Natural History of Diptera. In Manual of afrotropical Diptera. Volume 1. Introductory chapters and keys to Diptera families (eds Kirk-Spriggs A.H. and Sinclair B.J.) pp. 135-152*. Suricata 4. South African National Biodiversity Institute, Pretoria.

Lambkin, C. L., Sinclair, B. J., Pape, T., Courtney, G. W., Skevington, J. H., Meier, R., Yeates, D. K., Blagoderov, V., and Wiegmann, B. M. (2013). The phylogenetic relationships among infraorders and superfamilies of diptera

based on morphological evidence. *Systematic Entomology*, 38(1):164–179.

Le Roy, C., Amadori, D., Charberet, S., Windt, J., Muijres, F. T., Llaurens, V., and Debat, V. (2021). Adaptive evolution of flight in morpho butterflies. *Science*, 374(6571):1158–1162.

Le Roy, C., Tervelde, N., Engels, T., and Muijres, F. T. (2025). Adaptations in wing morphology rather than wingbeat kinematics enable flight in small hoverfly species. *eLife*, 13.

Lehmann, F.-O. and Dickinson, M. H. (1997). The changes in power requirements and muscle efficiency during elevated force production in the fruit fly drosophila melanogaster. *Journal of Experimental Biology*, 200(7):1133–1143.

Lehmann, F.-O. and Dickinson, M. H. (1998). The control of wing kinematics and flight forces in fruit flies (drosophila spp.). *Journal of Experimental Biology*, 201(3):385–401.

Lighthill, M. J. (2001). *Waves in fluids*. Cambridge university press.

Liu, Y., Liu, L., and Sun, M. (2024). Power requirements in hovering flight of mosquitoes. *Physics of Fluids*, 36(2).

Lyu, Y. Z. and Sun, M. (2021). Power requirements for the hovering flight of insects with different sizes. *Journal of insect physiology*, 134:104293.

Lyu, Y. Z., Zhu, H. J., and Sun, M. (2019). Aerodynamic forces and vortical structures of a flapping wing at very low reynolds numbers. *Physics of Fluids*, 31(4).

McLachlan, A. and Neems, R. (1996). Is flight architecture determined by physical constraints or by natural selection?: the case of the midge chironomus plumosus. *Journal of Zoology*, 240(2):301–308.

Melis, J. M., Siwanowicz, I., and Dickinson, M. H. (2024). Machine learning reveals the control mechanics of an insect wing hinge. *Nature*, pages 1–9.

Morgan, K. R. and Shelly, T. E. (1988). Body temperature regulation in desert robber flies (diptera: Asilidae). *Ecological Entomology*, 13(4):419–428.

Muijres, F. T. (2023). Quantifying and analyzing mosquito movement from video tracking results. *Cold Spring Harbor Protocols*, 2023(2):pdb–prot107929.

Muijres, F. T., Chang, S. W., van Veen, W. G., Spitzen, J., Biemans, B. T., Koehl, M. A., and Dudley, R. (2017a). Escaping blood-fed malaria mosquitoes minimize tactile detection without compromising on take-off speed. *Journal of Experimental Biology*, 220(20):3751–3762.

Muijres, F. T., Elzinga, M. J., Melis, J. M., and Dickinson, M. H. (2014). Flies evade looming targets by executing rapid visually directed banked turns. *Science*, 344(6180):172–177.

Muijres, F. T., Iwasaki, N. A., Elzinga, M. J., Melis, J. M., and Dickinson, M. H. (2017b). Flies compensate for unilateral wing damage through modular adjustments of wing and body kinematics. *Interface Focus*, 7(1):20160103.

Nalbach, G. (1993). The halteres of the blowfly calliphora: I. kinematics and dynamics. *Journal of Comparative Physiology A*, 173:293–300.

Nath, T., Mathis, A., Chen, A. C., Patel, A., Bethge, M., and Mathis, M. W. (2019). Using deeplabcut for 3d markerless pose estimation across species and behaviors. *Nature protocols*, 14(7):2152–2176.

Nedunchezian, K., Kang, C.-k., and Aono, H. (2019). Effects of flapping wing kinematics on the aeroacoustics of hovering flight. *Journal of Sound and Vibration*, 442:366–383.

Nicholson, D. B., Ross, A. J., and Mayhew, P. J. (2014). Fossil evidence for key innovations in the evolution of insect diversity. *Proceedings of the Royal Society B: Biological Sciences*, 281(1793):20141823.

Nielsen, E. T. and Haeger, J. S. (1960). Swarming and mating in mosquitoes. In *Swarming and Mating in Mosquitoes*, volume 1, page 72. BioOne.

Norberg, U. (2007). Flight and scaling of flyers in nature. *Flow phenomena in nature*, 1:120–154.

Norberg, U. M. (1996). *Energetics of flight*, pages 199–249. Springer.

Pélabon, C., Firmat, C., Bolstad, G. H., Voje, K. L., Houle, D., Cassara, J., Rouzic, A. L., and Hansen, T. F. (2014). Evolution of morphological allometry. *Annals of the new York Academy of Sciences*, 1320(1):58–75.

Pennetier, C., Warren, B., Dabiré, K. R., Russell, I. J., and Gibson, G. (2010). "singing on the wing" as a mechanism for species recognition in the malarial mosquito anopheles gambiae. *Current Biology*, 20(2):131–136.

Phan, H. V. and Park, H. C. (2018). Wing inertia as a cause of aerodynamically uneconomical flight with high angles of attack in hovering insects. *Journal of Experimental Biology*, 221(19):jeb187369.

Polilov, A. A. (2015). Small is beautiful: features of the smallest insects and limits to miniaturization. *Annual review of entomology*, 60(1):103–121.

Ratnasingham, S. and Hebert, P. D. (2007). Bold: The barcode of life data system (http://www. barcodinglife. org). *Molecular ecology notes*, 7(3):355–364.

Rayner, J. M. (1988). *Form and function in avian flight*, pages 1–66. Springer.

Revell, L. J. (2012). phytools: an r package for phylogenetic comparative biology (and other things). *Methods in ecology and evolution*, 3:217–223.

Riskin, D. K., Iriarte-Díaz, J., Middleton, K. M., Breuer, K. S., and Swartz, S. M. (2010). The effect of body size on the wing movements of pteropodid bats, with insights into thrust and lift production. *Journal of Experimental Biology*, 213(23):4110–4122.

Rohlf, F. J. (2015). The tps series of software. *Hystrix*, 26(1):1–4.

Rohlf, F. J. and Slice, D. (1990). Extensions of the procrustes method for the optimal superimposition of landmarks. *Systematic Biology*, 39(1):40–59.

Rohner, P. T. (2020). Evolution of multivariate wing allometry in schizophoran flies (diptera: Schizophora). *Journal of Evolutionary Biology*, 33(6):831–841.

Sane, S. P. (2003). The aerodynamics of insect flight. *Journal of Experimental Biology*, 206(23):4191–4208.

Schindelin, J., Arganda-Carreras, I., Frise, E., Kaynig, V., Longair, M., Pietzsch, T., Preibisch, S., Rueden, C., Saalfeld, S., Schmid, B., et al. (2012). Fiji: an open-source platform for biological-image analysis. *Nature methods*, 9(7):676–682.

Schlichting, H. and Gersten, K. (2016). *Boundary-layer theory*. springer.

Seo, J.-H., Hedrick, T. L., and Mittal, R. (2019). Mechanism and scaling of wing tone generation in mosquitoes. *Bioinspiration & biomimetics*, 15(1):016008.

Skowron Volponi, M. A., McLean, D. J., Volponi, P., and Dudley, R. (2018). Moving like a model: mimicry of hymenopteran flight trajectories by clearwing moths of southeast asian rainforests. *Biology Letters*, 14(5):20180152.

Srygley, R. and Thomas, A. L. (2002). Unconventional lift-generating mechanisms in free-flying butterflies. *Nature*, 420(6916):660–664.

Srygley, R. B. and Dudley, R. (1993). Correlations of the position of center of body mass with butterfly escape tactics. *Journal of Experimental Biology*, 174(1):155–166.

Symonds, M. R. and Blomberg, S. P. (2014). A primer on phylogenetic generalised least squares. *Modern phylogenetic comparative methods and their application in evolutionary biology: concepts and practice*, pages 105–130.

Tercel, M. P., Veronesi, F., and Pope, T. W. (2018). Phylogenetic clustering of wingbeat frequency and flight-associated morphometrics across insect orders. *Physiological Entomology*, 43:149–157.

Theriault, D. H., Fuller, N. W., Jackson, B. E., Bluhm, E., Evangelista, D., Wu, Z., Betke, M., and Hedrick, T. L. (2014). A protocol and calibration method for accurate multi-camera field videography. *Journal of Experimental Biology*, page jeb. 100529.

Ulrich, W. and Szpila, K. (2008). Body size distributions of eastern european diptera. *Polish Journal of Ecology*, 56(4):557–568.

Wardill, T. J., Fabian, S. T., Pettigrew, A. C., Stavenga, D. G., Nordström, K., and Gonzalez-Bellido, P. T. (2017). A novel interception strategy in a miniature robber fly with extreme visual acuity. *Current Biology*, 27(6):854–859.

Wiegmann, B. M., Trautwein, M. D., Winkler, I. S., Barr, N. B., Kim, J.-W., Lambkin, C., Bertone, M. A., Cassel, B. K., Bayless, K. M., Heimberg, A. M., et al. (2011). Episodic radiations in the fly tree of life. *Proceedings of the National Academy of Sciences*, 108(14):5690–5695.

Wiegmann, B. M. and Yeates, D. K. (2017). *Phylogeny of Diptera. In Manual of afrotropical Diptera. Volume 1. Introductory chapters and keys to Diptera families (eds Kirk-Spriggs A.H. and Sinclair B.J.) pp. 253-265*. Suricata 4. South African National Biodiversity Institute, Pretoria.

Willmott, A. P. and Ellington, C. P. (1997). The mechanics of flight in the hawkmoth manduca sexta. i. kinematics of hovering and forward flight. *Journal of Experimental Biology*, 200(21):2705–2722.

Wishart, G. and Riordan, D. (1959). Flight responses to various sounds by adult males of aedes aegypti (l.)(diptera: Culicidae) 1. *The Canadian Entomologist*, 91(3):181–191.

Yarger, A. M., Jordan, K. A., Smith, A. J., and Fox, J. L. (2021). Takeoff diversity in diptera. *Proceedings of the Royal Society B*, 288(1942):20202375.

Yeates, D. K. and Wiegmann, B. M. (2005). *The evolutionary biology of flies*. Columbia University Press.

Yeates, D. K., Wiegmann, B. M., Courtney, G. W., Meier, R., Lambkin, C., and Pape, T. (2007). Phylogeny and systematics of diptera: two decades of progress and prospects. *Zootaxa*, 1668(1):565–590.

FIGURES

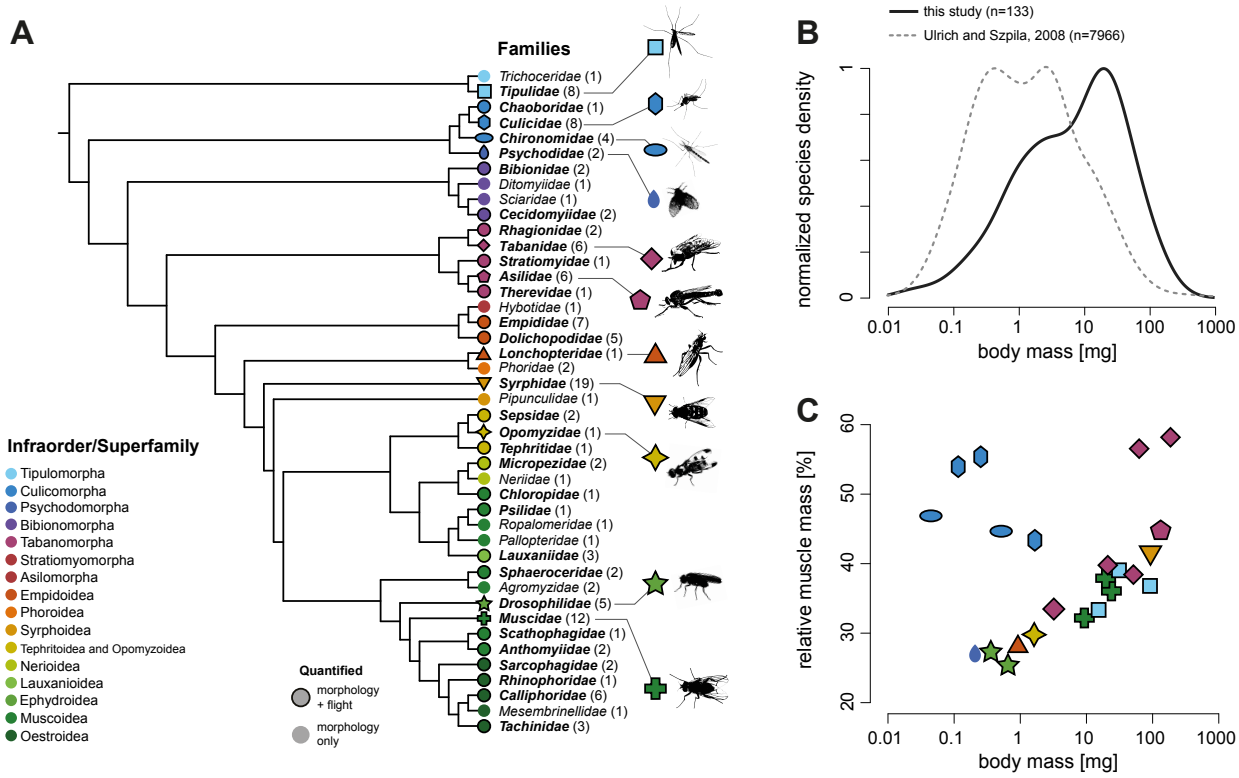

Figure 1. **Phylogeny and morphology of the 133 studied Dipteran species**. (**A**) The studied Diptera families shown with their phylogenetic relationships; the number of studied species for each family are given in parentheses. The families for which flight was quantified in at least one species are highlighted with black outlines. Phylogeny was obtained from Wiegmann and Yeates (2017). (**B**) Distribution of body mass in the sampled species (continuous black line) overlaid with a representative distribution of body mass across most Diptera (dashed grey line), estimated from a large meta-analysis covering nearly 8,000 species (Ulrich and Szpila, 2008) . (**C**) Relative muscle mass *versus* body mass in a subset of species broadly spanning the phylogeny. The data points match non-circle symbols in (**A**). Species are colored by infraorder and/or superfamily to provide a clear overview of phylogenetic position. These groupings were chosen for visualization purposes and do not imply equivalent taxonomic rank.

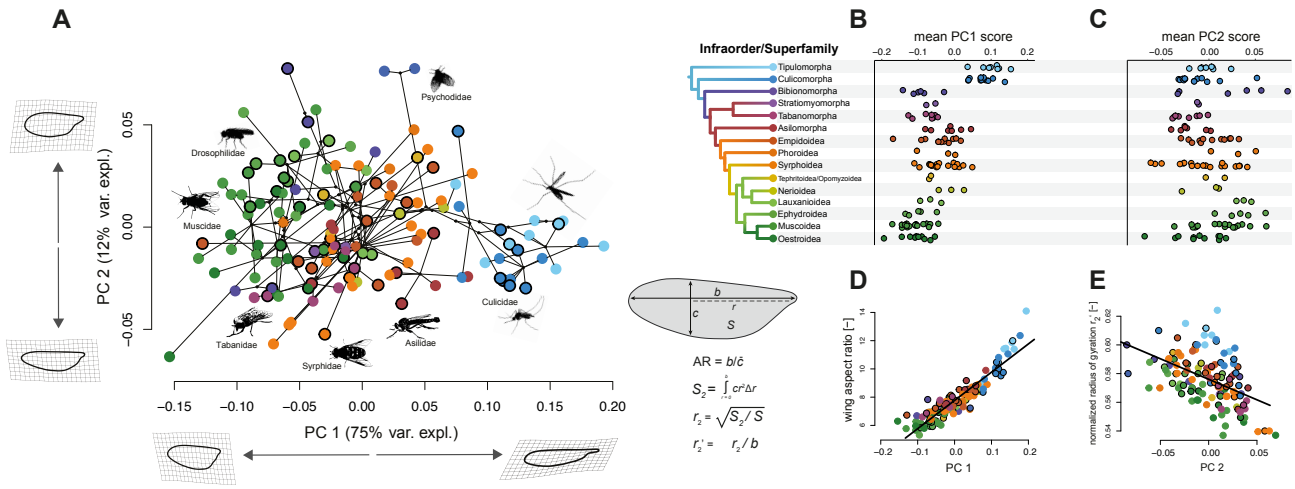

Figure 2. **Wing shape variation across Diptera, quantified using a Principal Component Analysis (PCA)**.(**A**) The two first principal components (PC1 and PC2), together with the associated shape changes and percentage of the variation explained by the principal components. Shown wing shapes represent the extreme values associated with each PC axis. Each data point shows a species-average wing shape. Species for which flight was quantified are highlighted with black circles. (**B-C**) PC1 was strongly structured by phylogeny, while PC2 showed a weaker phylogenetic signal. (**D-E**) The two functional shape descriptors — aspect ratio (AR) and normalized second-radius-of-gyration (r_2^*) — were most strongly associated with PC1 and PC2, respectively.

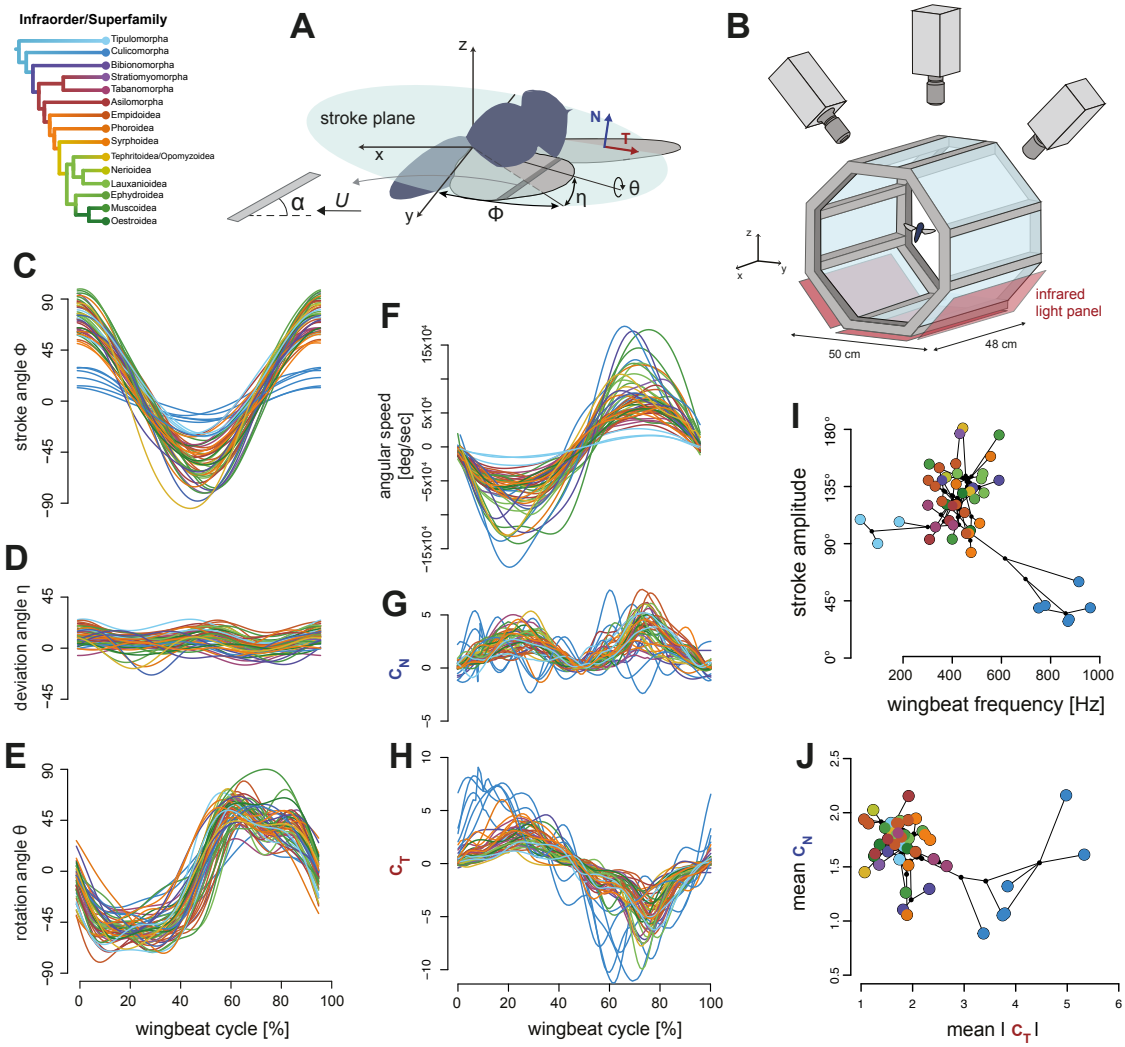

Figure 3. **Wingbeat kinematics and aerodynamics of the 46 Diptera species studied in flight**. (**A**) The wingbeat kinematics are defined by the temporal dynamics of the parameters: wing stroke angle within the stroke plane (ϕ); wing deviation angle out of the stroke plane (η); wing rotation angle along the spanwise axis (θ); air velocity vector relative to the wing (U); angle-of-attack of the wing (α). Aerodynamic forces on each wing were estimated using computational fluid dynamics (CFD), and defined as the force coefficients normal and tangential to the stroke-plane (N and T, respectively). (**B**) For the flight experiments, flies were released in an octagon-shaped flight arena. We recorded stereoscopic high-speed videos of the flying flies using three synchronized high-speed video cameras; from the videos we reconstructed the three-dimensional body and wingbeat kinematics. Infrared light panels positioned as the bottom of the arena enabled high contrast between the flying insect and the background. (**C-H**) Temporal dynamics of the wingbeat kinematics and aerodynamics throughout a single wingbeat cycle, for the 46 flying Diptera species (video S1). Each line represents a species-averaged temporal dynamic, color-coded by infraorder (top left). (**C-E**) Temporal dynamics of the three wingbeat kinematics angle (stroke, deviation, and rotation angle, respectively). (**F**) Angular speed throughout the wingbeat cycle. (**G,H**) Aerodynamic force coefficients normal and tangential to the stroke plane, respectively. (**I,J**) Wingbeat-average kinematics and aerodynamics for the 46 Diptera species studied in flight. Data points show average data per species, are color-coded by infraorder, and are connected based on phylogeny (see top left). (**I**) Stroke amplitude versus wingbeat frequency for the 46 species-averaged wingbeats. (**J**) Wingbeat-average force coefficient normal to the stroke-plane versus the equivalent absolute tangential force coefficient.

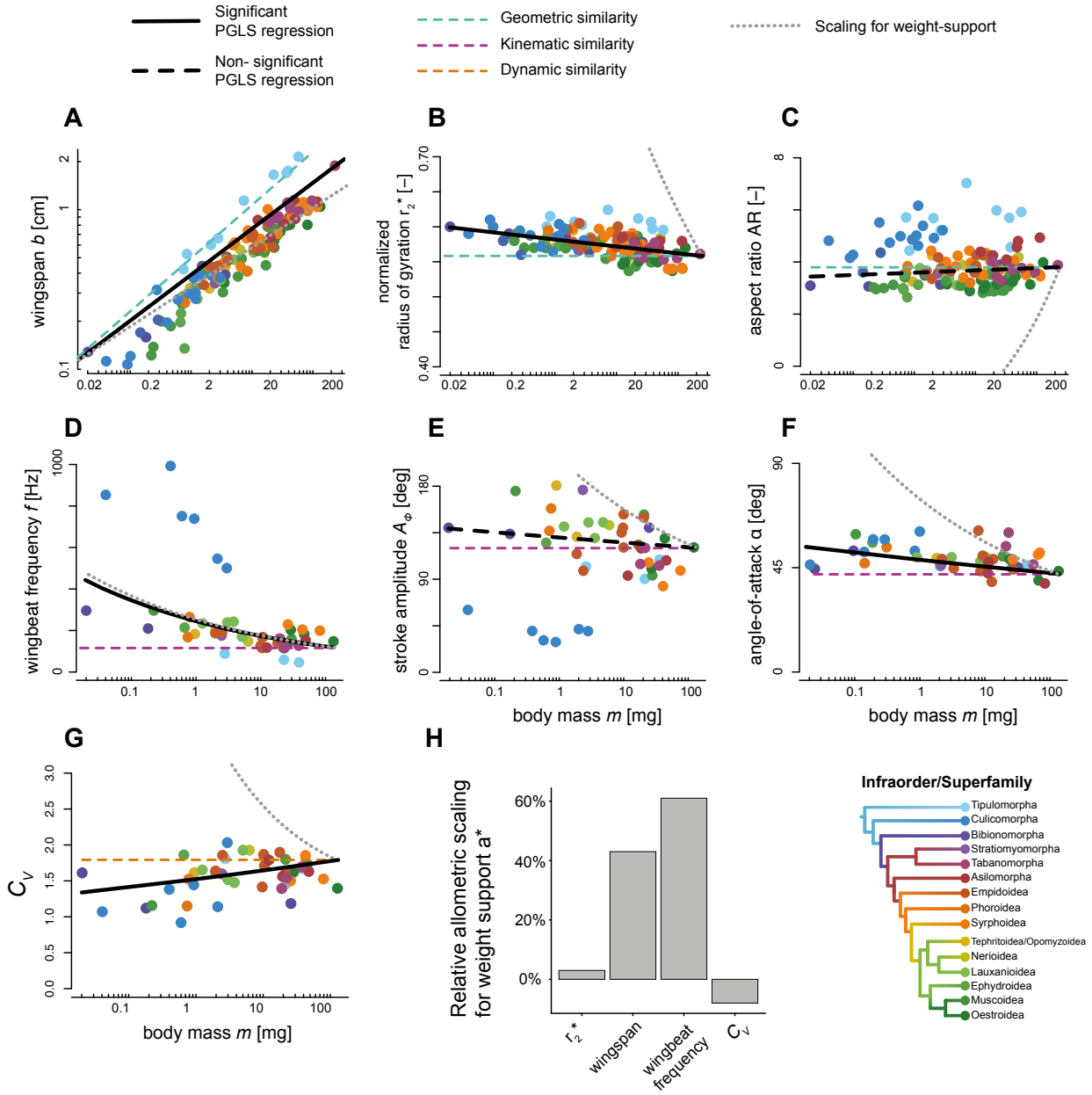

Figure 4. **Scaling of morphology, wingbeat kinematic and aerodynamics with body mass**. (**A-G**) Relationship between morphological, kinematics and aerodynamics parameters from the aerodynamic force model (Eqn 3) and body mass. Data points show species-average results, and are color-coded by infraorder (see bottom right). The best-fitting line from the PGLS regression on the data is shown as a black line; the trend line is solid when the parameter varies significantly with body mass, or dashed when the relationship is not significant. Expected slopes under geometric, kinematic, and dynamic similarity are shown as blue, purple, and orange dashed lines, respectively. The expected scaling for maintaining weight support (assuming all other parameter scaling isometrically) is shown as a grey dashed line. All plots are displayed on a linear–log scale, except for wingspan, which is shown on a log–log scale. (**H**) Relative contributions of the different parameters to maintaining weight support across sizes.

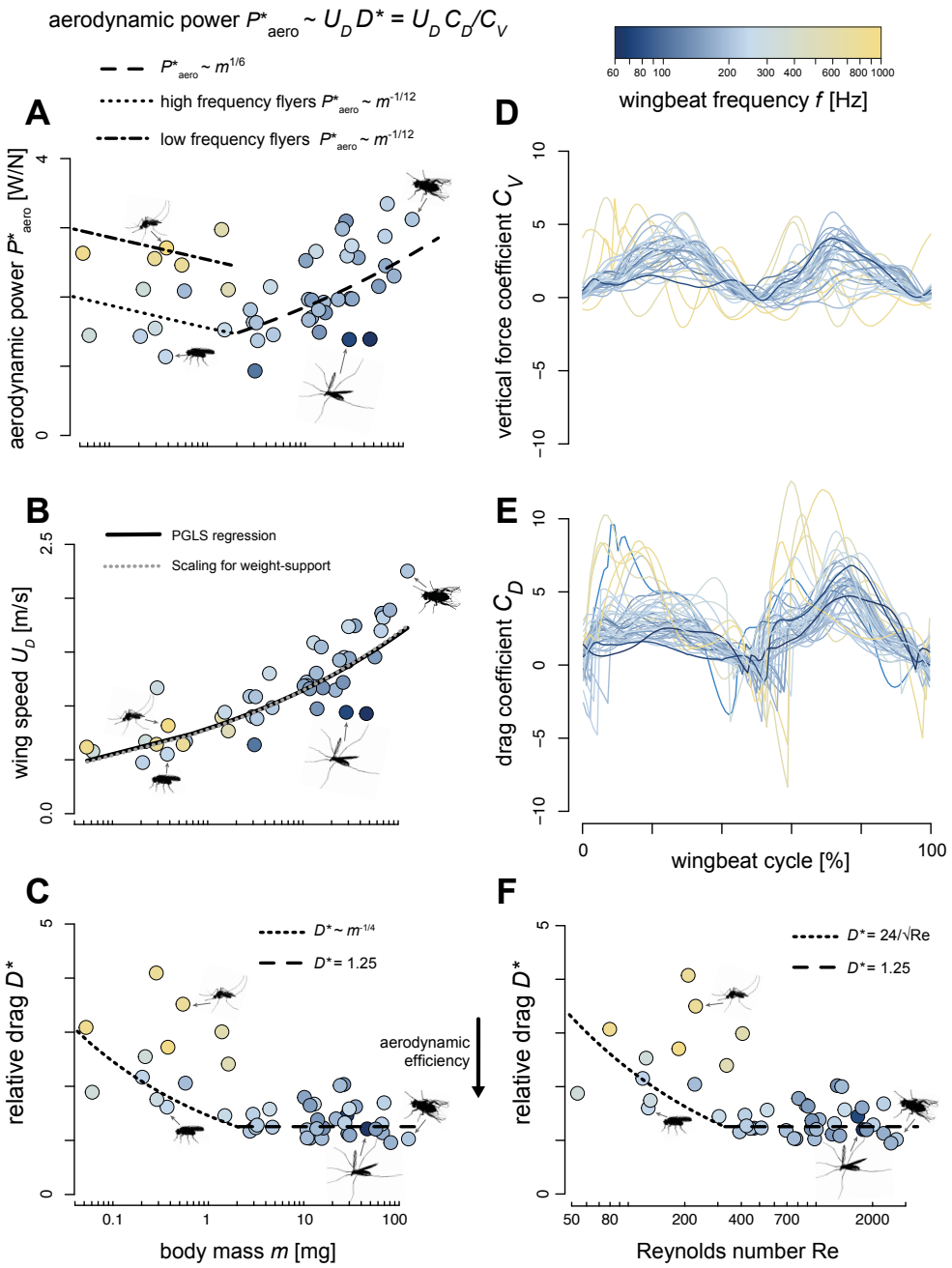

Figure 5. **Scaling of aerodynamic power with body mass and Reynolds number**. Data points and colored lines show species-average results, and are color-coded with wingbeat frequency (see top right). Trend lines show fits based on physical and aerodynamic scaling laws and PGLS regression. (**A-C**) Scaling of normalized aerodynamic power with body mass, and that of the sub-components wing speed and relative drag, respectively ($P^* \sim U_D\, D^*$). (**A**) Aerodynamic power increases with body mass in Diptera species heavier than 2 mg, but decreases with mass in smaller species ($m < 2$ mg). Species with higher wingbeat frequencies show elevated power requirements. (**B**) The increase in power with body mass for large Diptera is primarily driven by increasing wing speed, which scales as $U_D \sim m^{1/6}$. (**C**) Relative drag (D^*) remains approximately constant for large Diptera, while it increases with decreasing body mass in species under 2 mg, and is exceptionally high in high frequency fliers. (**D,E**) The temporal dynamics of the vertical force coefficient and drag coefficient for all studied species. Relative drag equals the ratio of these coefficients ($D^* = C_D/C_V$), and these data therefore show that the increase in relative drag in high frequency fliers is primarily due to an increase in the drag coefficient. (**F**) The scaling of relative drag with Reynolds number suggest that the increased relative drag for tiny flying Diptera ($m < 2$ mg) is caused by the enhanced viscous effects at Reynolds numbers below 400.

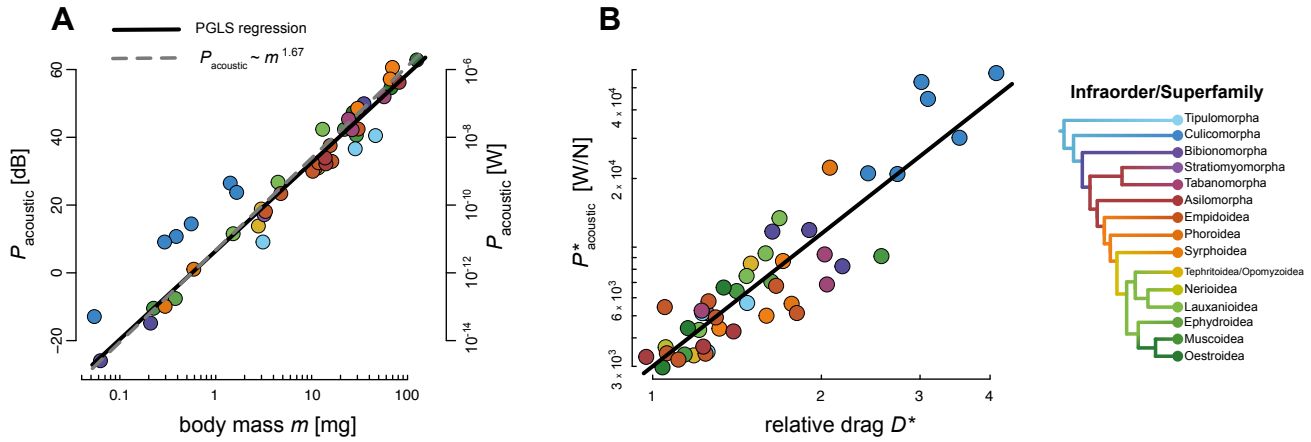

Figure 6. **Scaling of aeroacoustic power with body mass and aerodynamic drag production**. Data points show species-average results, and are color-coded by infraorder (see right). The black solid lines and grey dashed line show significant PGLS regressions and the theoretical scaling, respectively. (**A**) Aerocoustic power increases with body mass across Diptera, with Culicomorpha species exhibiting enhanced acoustic power compared to other Diptera group of similar sizes. The PGLS regression (solid black line) closely matches the theoretical scaling expectation $P_{\text{acoustic}} \sim m^{1.67}$ (dashed grey line). (**B**) Normalized acoustic power (P^*_{acoustic}) scales positively with the relative aerodynamic drag (D^*), whereby Culicomorpha produce both highest normalized sound power and relative drag.

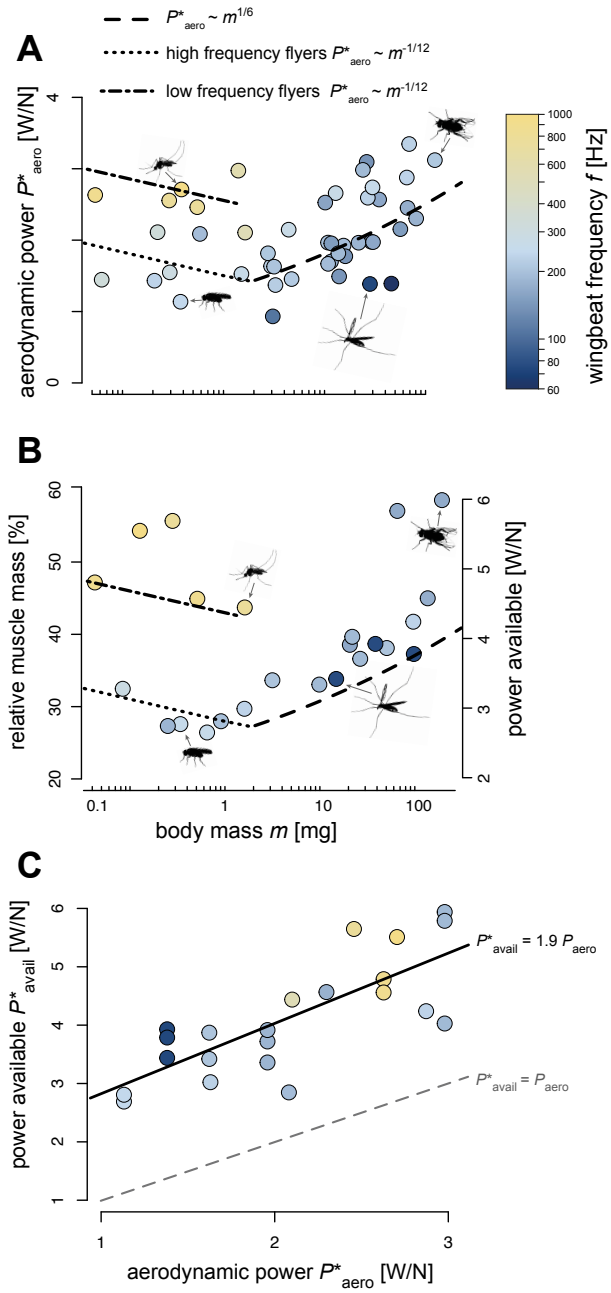

Figure 7. **Scaling of aerodynamic power and musculature-based available power**. Data points show results per species, and are color-coded with wingbeat frequency (top right). Trend lines are based on scaling laws (see Fig. 5) and a statistical fit. (**A**) Aerodynamic power requirement (same panel as Fig. 5A) aligns with the scaling of available flight power (**B**), estimated from thorax mass in a subset of 22 species. Points in **A** represent species means, whereas points in **B** represent individual measurements. (**C**) Required aerodynamic power versus available power. The solid black and dashed grey lines shows the best OLS fit on the data, and for equal required and available power ($P^*_{\text{avail}} = P^*_{\text{aero}}$), respectively. On average, Diptera possess approximately a two-fold higher available power than the aerodynamic power required for flight.

1106 **TABLES**

Table 1. Results of phylogenetic general least square (PGLS) regressions of wing morphology, wingbeat kinematics and aerodynamic parameters (from aerodynamic model, see Eqn 3) on body mass. Stars indicated % confidence intervals excluding the isometry slope, suggesting allometry.

	n	P	R^2 (%)	Intercept	Scaling factor estimate [95% C.I.]	Scaling factor for similarity	Scaling factor for single-metric weight support	Allometry
Wing morphology								
Wingspan b	133	**<0.001**	81.94	-0.408	**0.289 [0.266 – 0.313] ***	1/3 = 0.33	1/4 = 0.25	**negative**
Normalized radius of gyration r_2*	133	**<0.001**	16.59	-0.227	**-0.007 [-0.011 – -0.004] ***	0	-1/6 = 0.17	**negative**
Wing aspect ratio AR	133	0.188	1.32	0.637	0.009 [-0.004 – 0.024]	0	1/3 = 0.33	isometry
Wingbeat kinematics								
Wingbeat frequency f	46	<0.001	37.57	2.307	-0.149 [-0.207 – -0.091] *	0	-1/6 = 0.17	**negative**
Stroke amplitude A_ϕ	46	0.677	0.1	1.976	-0.011 [-0.038 – 0.058]	0	-1/6 = 0.17	isometry
Wing speed U_r	46	**<0.001**	66.77	-0.107	0.167 [0.132 – -0.201] *	1/3 = 0.33	1/6 = 0.17	-
Aerodynamics								
Vertical force coefficient C_V	46	0.013	13.11	0.169	0.033 [0.007 – 0.059]	0	-1/3 = 0.33	**positive**

SUPPLEMENTARY FIGURES

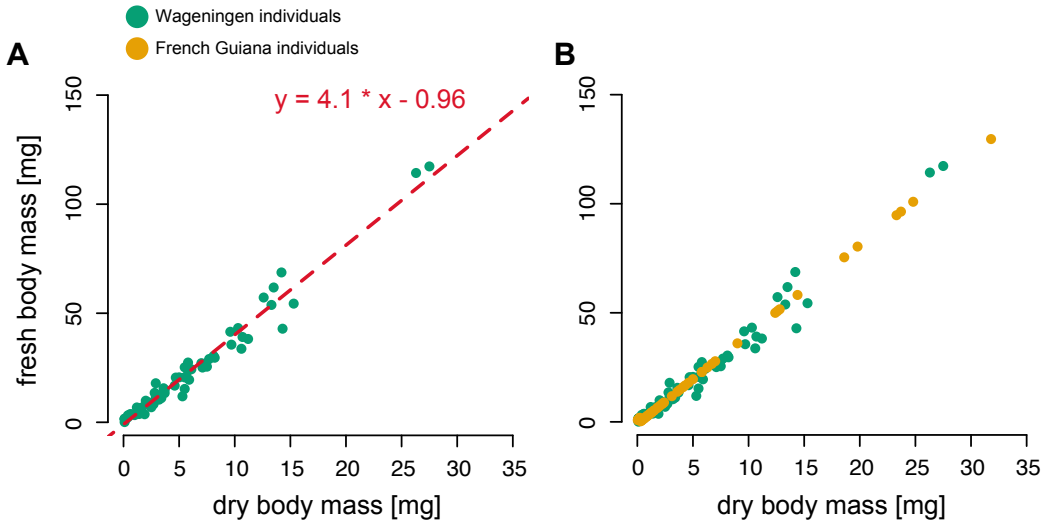

Figure S1. The fresh body mass of specimens collected in French-Guiana was approximated using the relationship between dry and the fresh body mass among specimens collected in Wageningen. (**A**) A linear regression model was fitted to the data from Wageningen. (**B**) The equation of the fitted model was used to estimate fresh body mass: $m = 4.1 * m_{\text{dry}} - 0.96$.

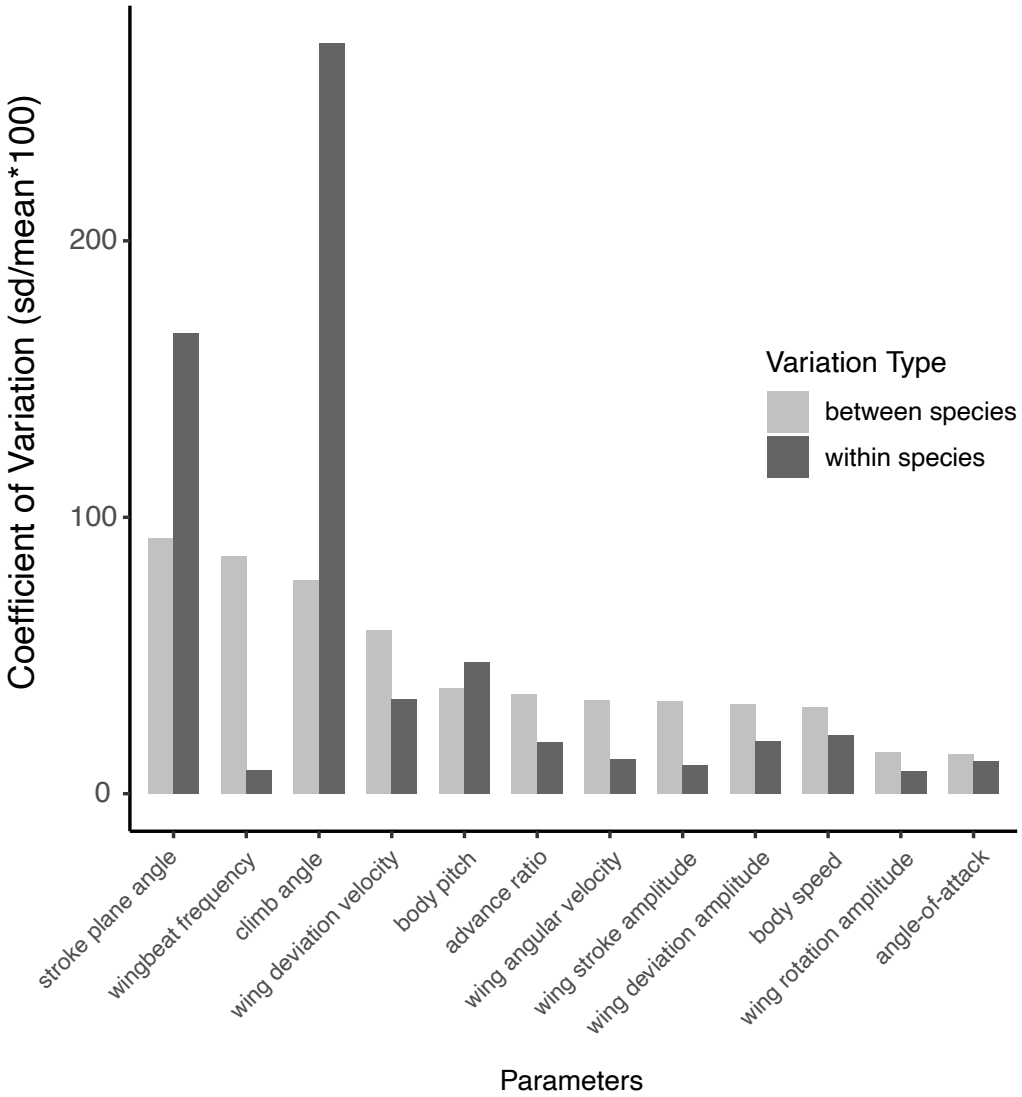

Figure S2. Intra-specific versus inter-specific variation in flight kinematics parameters assessed with the coefficient of variation (CV). Parameters are ordered by decreasing inter-specific CV.

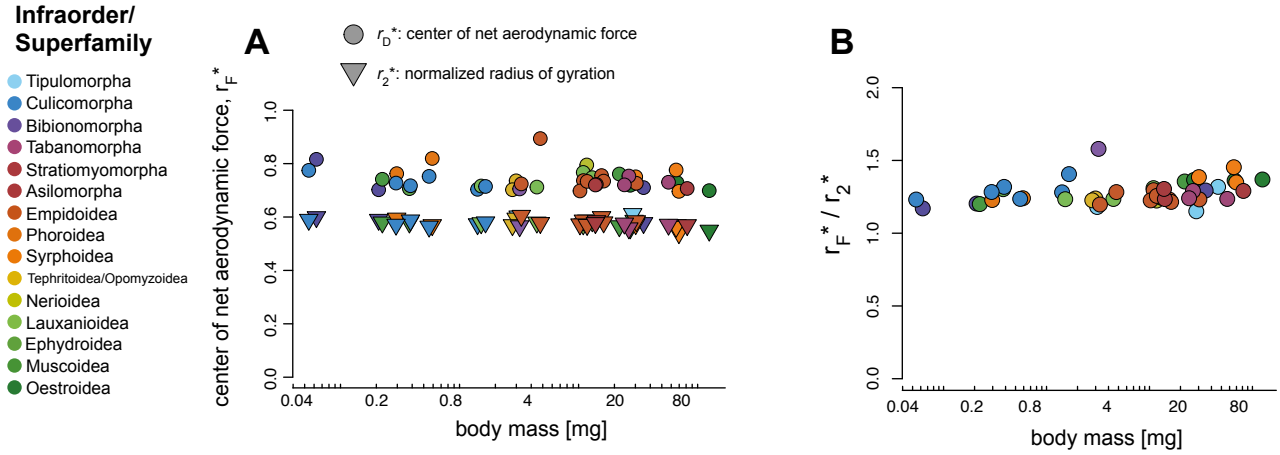

Figure S3. Comparison between normalized radius of gyration r_2^* and center of the aerodynamic drag force r_D^*.

SUPPLEMENTARY TABLES

Table S1. Phylogenetic signal in morphological and wingbeat kinematic parameters, computed using Blomberg's K. Bold indicates significant p-value (< 0.05).

Wing morphology			**Wingbeat kinematics**		
Parameters	K	*P*	**Parameters**	K	*P*
Wingspan b	0.215	**0.001**	Wingbeat frequency f	0.611	**0.002**
Wing area S	0.142	**0.026**	Stroke amplitude A_ϕ	0.472	**0.001**
Mean wing chord $\bar{c}$	0.214	**0.005**	Wing angular velocity $\overline{\omega}$	0.401	**0.006**
Wing radius of gyration r_2	0.107	0.202	Wing angle-of-attack $\overline{\alpha}$	0.166	0.229
Normalized wing radius of gyration r_2*	0.246	**0.001**			
Wing aspect ratio AR	0.698	**0.001**			
Body mass m	0.106	0.123			

Table S2. Comparison of sum of squares from nested ANOVAs accounting for multiple flight sequence replicates per species.

Parameters	between-species sum of square	within-species sum of square	largest source of variation
Wingbeat frequency	4.48×10^{6}	7.14×10^{4}	between-species
Stroke amplitude	1.64×10^{5}	1.15×10^{4}	between-species
Rotation amplitude	3.52×10^{4}	8.61×10^{3}	between-species
Deviation amplitude	2.53×10^{3}	8.29×10^{2}	between-species
Wing angular velocity	4.69×10^{10}	7.53×10^{9}	between-species
Angle-of-attack	4.57×10^{3}	2.81×10^{3}	between-species
Stroke plane angle	1.59×10^{4}	2.12×10^{4}	within-species
Climb angle	3.11×10^{4}	3.42×10^{4}	within-species
Body pitch	1.59×10^{4}	2.12×10^{4}	within-species
Body speed	6.28×10^{0}	3.00×10^{0}	between-species

SUPPLEMENTARY VIDEO LEGEND

Video S1. Collage of high-speed videos of all 46 Diptera species studied in flight. The separate videos have been scaled and aligned such that they fit the collage and video duration, and thus spatial and temporal scales differ between them. The corresponding full videos are available in the digital repository (see Data Availability Statement).